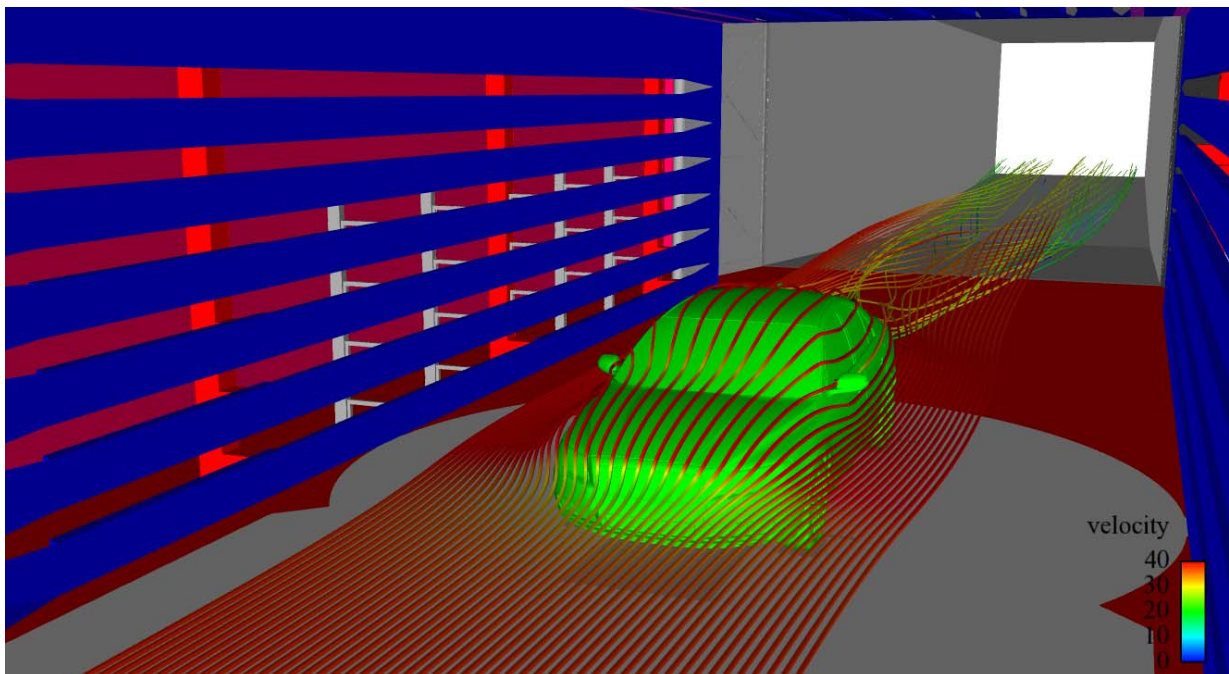


CHALMERS



CFD Simulation of the Volvo Cars Slotted Walls Wind Tunnel

Master's Thesis in Solid and Fluid Mechanics

MATTIAS OLANDER

Department of Applied Mechanics
Division of Division of Vehicle Engineering and Autonomous Systems
CHALMERS UNIVERSITY OF TECHNOLOGY
Göteborg, Sweden 2011
Master's Thesis 2011:33

CFD Simulation of the Volvo Cars Slotted Walls Wind Tunnel

Master's Thesis in Solid and Fluid Mechanics
MATTIAS OLANDER

Department of Applied Mechanics
Division of Division of Vehicle Engineering and Autonomous Systems
CHALMERS UNIVERSITY OF TECHNOLOGY

Göteborg, Sweden 2011

CFD Simulation of the Volvo Cars Slotted Walls Wind Tunnel
MATTIAS OLANDER

©MATTIAS OLANDER, 2011

Master's Thesis 2011:33
ISSN 1652-8557
Department of Applied Mechanics
Division of Division of Vehicle Engineering and Autonomous Systems
Chalmers University of Technology
SE-412 96 Göteborg
Sweden
Telephone: + 46 (0)31-772 1000

Cover:
Velocity streamlines around the S80 inside the PVT tunnel

Chalmers Reproservice
Göteborg, Sweden 2011

CFD Simulation of the Volvo Cars Slotted Walls Wind Tunnel
Master's Thesis in Solid and Fluid Mechanics
MATTIAS OLANDER
Department of Applied Mechanics
Division of Division of Vehicle Engineering and Autonomous Systems
Chalmers University of Technology

Abstract

When CFD simulations are performed at Volvo Cars, a case which resembles the condition for a car traveling on a open road is simulated. The results from these simulations have often proved to be different compared to the results from the experiments in the Volvo Cars slotted walls wind tunnel. To investigate the reason behind these differences a number of CFD simulations of the Volvo Cars wind tunnel have been performed. The simulations have been focused on three main cases, empty tunnel, tunnel with a simplified S60 and tunnel with a detailed S80. The results have been compared to ordinary CFD simulations and to newly made experiments in the wind tunnel. The flow produced by the numerical simulations in the empty wind tunnel has proved to be largely asymmetric due to the asymmetric geometry of the slotted walls' support structure. This has greatly affected the flow around a car in the tunnel resulting in a different flow field compared to the standard CFD simulation. The drag and lift coefficient of the S60 and S80 have been lower in the CFD simulations of the wind tunnel compared to the ordinary CFD simulations, which is the opposite to what have been found when comparing the standard CFD simulations to the real experiments in the tunnel. The reason behind this is believed to be mainly due to the geometry simplifications of the simulated tunnel and the uniform inlet boundary condition, which have resulted in a very much more uniform flow in the CFD simulations compared to the experiments.

Keywords: CFD, Wind Tunnel, Slotted Walls, Mesh, Wind loads, Aerodynamics, Volvo Cars, Experiment

Contents

Abstract	I
Contents	III
Preface	V
List of Abbreviations	VI
1 Introduction	1
1.1 Background	1
1.2 Purpose	1
1.3 Goal	1
1.4 Limitations	1
1.5 Method	1
2 Background	3
2.1 The Volvo Cars Slotted Walls Wind Tunnel - PVT	3
2.2 The Standard CFD Procedure at Volvo Cars	5
3 Theory	7
3.1 The Governing Equations	7
3.2 The Near Wall Flow	7
4 Method	9
4.1 Geometry	9
4.1.1 PVT Tunnel	9
4.1.2 S60	11
4.1.3 S80 Closed Front	12
4.1.4 S80 Open Cooling	13
4.2 Mesh	14
4.2.1 PVT Tunnel	14
4.2.2 S60	15
4.2.3 S80 Closed Front	16
4.2.4 S80 Open Cooling	17
4.3 Calculation Settings	18
4.3.1 Empty Tunnel	21
4.3.2 Tunnel With Simple S60	21
4.3.3 Tunnel With S80 Closed Front	22
4.3.4 Tunnel With S80 Open Cooling	22
4.4 Postprocessing	22
5 Results and Discussion	24
5.1 Empty Tunnel	24
5.1.1 Asymmetrical Behaviour	24
5.1.2 Axial pressure gradient	26
5.1.3 Nozzle Contraction	26
5.1.4 Comparison With Experiments	28
5.2 Tunnel With Simplified S60	33
5.2.1 Asymmetrical Behaviour	33
5.2.2 PVT Tunnel impact on pressure coefficients	37

5.3	Tunnel With S80 Closed Front	39
5.3.1	Asymmetrical Behaviour	39
5.3.2	PVT Tunnel impact on pressure coefficients	42
5.3.3	Comparison With Experiments	48
5.4	Tunnel With S80 Open Cooling	49
5.4.1	PVT Tunnel impact on pressure coefficients	49
5.4.2	Comparison With Experiments	49
6	Conclusions	51
7	Recommendations and Future Work	52
	References	53

Preface

This master thesis has been performed at the Group at Volvo Cars in collaboration with the Department of Applied Mechanics, Chalmers University of Technology, Sweden, during the spring of 2011. Mattias Olander has been the student performing the master thesis with Simone Sebben as supervisor at Volvo Cars and Lennart Löfdahl as examiner at Chalmers.

Acknowledgement

I want to thank my supervisor at Volvo Cars, Simone Sebben, for her support and help with the CFD process during this master thesis. Without her this project would not have been possible to be realized. I want to thank Tim Walker for all the valuable discussions we have shared which have helped me tremendously. I also want to thank my examiner, Lennart Löfdahl for always being available whenever I had any questions regarding the project.

I want to thank thesis worker Erik Lindmark for assisting me when various geometries had to be created, for providing me with tips and tricks about the softwares used in this project and for the discussions we had. I want to thank CFD engineer Patrick Sondell whose help regarding softwares and other computer related issues have been deeply appreciated. I want to say thanks to CFD engineer Mattias Hejdesten for answering all my questions when Simone was not available. I also want to thank PhD student Lennart Sterken for enlighten me about micro drag and especially for picking me up at the airport, a big thanks!

Last I want to say thank you to the personnel at the PVT tunnel for lending me their time and energy and all the employees at the Volvo Cars aerodynamic department for the great atmosphere that I have experience during my time at Volvo Cars.

Göteborg June 2011
Mattias Olander

List of Abbreviations

CFD	Computational Fluid Dynamics
CAD	Computer Aided Design
PVT	Volvo Cars Slotted Walls Wind Tunnel
QUICK	Quadratic Upstream Interpolation for Convective Kinetics
BLCS	Boundary Layer Control System
GESS	Ground Effect Simulation System
WDU	Weel Drive Units
PID	Property ID
Aiolos	Company which upgraded and calibrated the wind tunnel

1 Introduction

1.1 Background

Today the exterior aerodynamic CFD simulations at Volvo Cars are performed with a virtual domain around the car, which has boundary conditions that resembles open road conditions, hence very different from the conditions of the Volvo Cars' slotted walls wind tunnel. In addition to that, the complete ground is set as moving in the CFD simulations which is a lot different from the advanced boundary layer control system and 5-belt moving ground system used in the wind tunnel. It is therefore complicated to compare the CFD results with the results from the wind tunnel as the two cases are very different from each other. Also, after the wind tunnel was upgraded in 2007, no extensive CFD simulation has been made on the wind tunnel, thus there exist no validity check of the CFD results.

1.2 Purpose

The purpose of this master thesis is to carry out extensive CFD simulations of the wind tunnel and to compare the results with results from both standard CFD simulations and real experiments in the wind tunnel, with the aim to be able to either verify the standard CFD simulations or explain the differences. The reasons behind certain results from the wind tunnel will be investigated and explained. The aim is also to get a better understanding of the flow field in the wind tunnel and to get a better picture of how the slotted walls affects the flow, especially with a car inside the tunnel.

1.3 Goal

The main goal of this master thesis understand the differences in flow field and forces between the standard CFD simulation and the wind tunnel results.

1.4 Limitations

The mesh will be limited to a maximum of approximate 100 million cells and the 3D-model of the wind tunnel is simplified to only include objects that are at least approximately 100 mm large, which means that small objects like for example cables are not modeled. The wind tunnel is only modeled from the start of the nozzle and to the end of the diffuser, hence the complete closed air-path that includes the bends and the main fan is not part of the model. The simulations will only be performed with the same main settings which is used in the standard procedure at Volvo Cars. This mean that, for example, only the realizable k-epsilon turbulence model will be used and no other turbulence model will be tested. In addition, all computations were performed in steady-state.

1.5 Method

The program ANSA will be used to clean up the CAD of the wind tunnel and prepare it for meshing. Before starting the meshing procedure the CAD is going to be compared to the real wind tunnel and if anything important is missing it will be added manually in ANSA. Harpoon will be used as mesher and Fluent to perform the calculations. The results will be exported to Enight for analysis and visualization. The first simulations will be performed on one half of the tunnel, with the boundary layer control system and the moving ground system turned of, just to ensure that the mesh is of good quality. The boundary layer control system will then be turned on step wise to make sure that the conservation of mass

through the domain is always satisfied. When successful simulations have been performed with the boundary control system in place, then the complete tunnel will be simulated and compared to the simulations performed on one half on the tunnel to distinguish if the flow is symmetrical. When the empty tunnel simulations are completed, a simple geometry of a S60 will be implemented in order to quickly investigate the complexity of simulations involving a car in the tunnel. The last step is then to put in a real car model of a S80 which will be possible to compare with the experiments.

2 Background

2.1 The Volvo Cars Slotted Walls Wind Tunnel - PVT

The construction of the Volvo Cars wind tunnel was completed in the mid 1980s and it was fully operational in 1986. It featured a horizontally closed air-path with a 6.6 m wide and 4.1 m high test section of slotted walls and ceiling, where the longitudinal slots created a 30% open-area ratio with the purpose of minimizing the blockage effects of the walls. The tunnel's closed air-path can be seen in Figure 2.1 which also shows parts of the slotted ceiling in the test section.

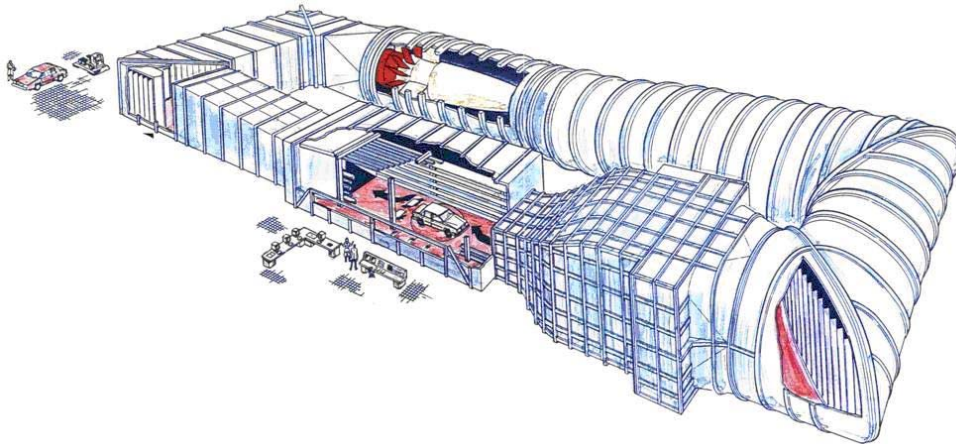


Figure 2.1: The Volvo Cars slotted walls wind tunnel

In 2006 the wind tunnel was upgraded to the specifications which it still has today in 2011. The upgrade included a complete moving ground system and a new boundary layer control system (BLCS). The fan power was increased from 2.3 MW to 5 MW to provide a wind speed of 250km/h in the test section.

The 5-belt moving ground system consist of a center belt and four wheel drive units (WDU) that can be moved to different positions depending on the vehicle's track width. The WDUs can be configured with three different belt widths, 280 mm, 360 mm and 410 mm and if necessary placed asymmetrically around the center belt.

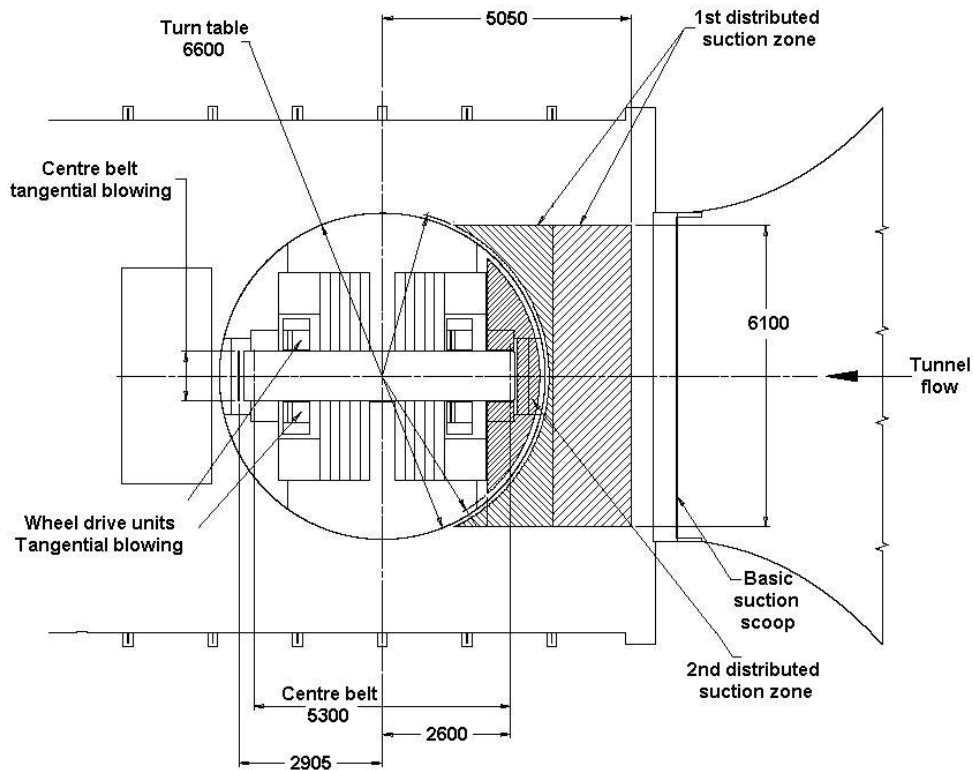


Figure 2.2: The layout of the floor

The BLCS consist of a boundary layer scoop situated just before the test section (basic scoop), floor mounted suction in front of the turn table in two steps(1st and 2nd suction) and tangential blowing behind the WDU and the center belt. The air removed by the basic scoop is inserted above the slotted ceiling in the direction of the flow by two ducts located at the front wall of the test section. The air removed by the 1st and 2nd suction is partially used for the tangential blowing while the rest is inserted on the right and left side of the front wall, behind the slotted walls. A schematically drawing of the moving ground system and boundary control system is showed in Figure 2.2.

The tunnel have three different configurations; Scoop only, Ground effects simulation system(GESS) off and Aerodynamic mode. For the Scoop only mode, only the basic scoop is operating with everything else turned off. In GESS off also the 1st and 2nd suction is turned on. For the Aerodynamic mode everything is activated.

The wind tunnel test section is not completely symmetric as four additional vertical support beams together with two horizontal beams are situated at the right side where the control room is housing. This is due to the slotted walls on the control room side having windows made of glass in order the make it possible to see through them. The additional support beams can be seen to the left in Figure 2.3, which shows the inside of the test section and the scale under the tunnel floor.

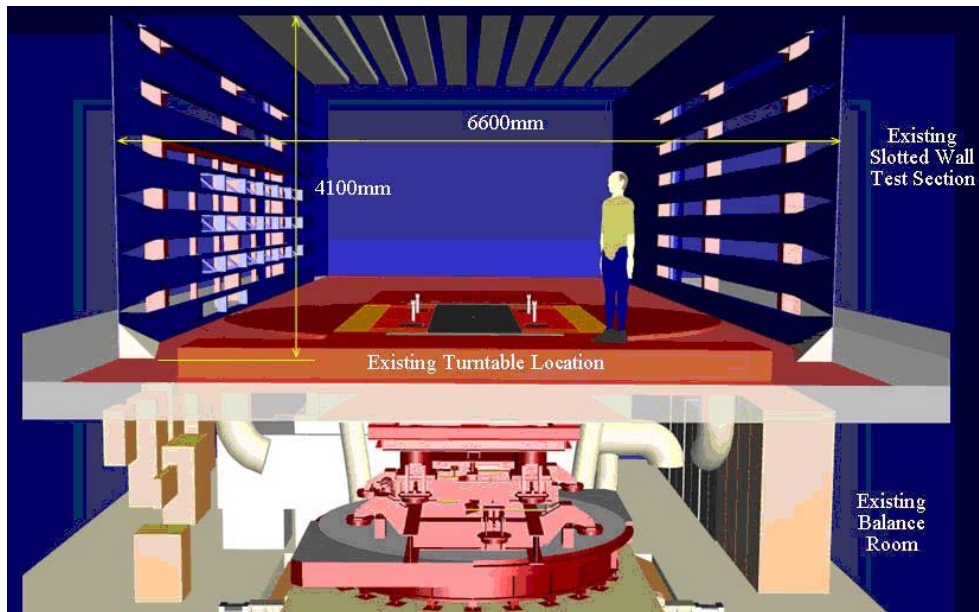


Figure 2.3: The slotted walls and the scale situated under the tunnel floor

For any further information regarding the upgrade of the PVT tunnel, see Ref. [1].

2.2 The Standard CFD Procedure at Volvo Cars

When CFD simulations are performed at Volvo Cars open road conditions are intended to be simulated. This is done by creating a large rectangular box around the car model representing the domain, which can be seen in Figure 2.4, and then applying symmetry wall conditions to the roof and side walls. A uniform velocity distribution is applied to the inlet and a zero pressure condition at the outlet.

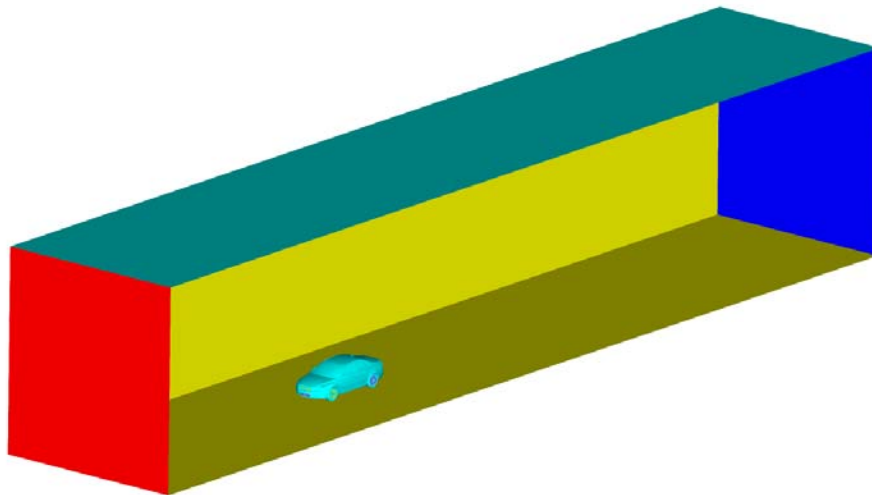


Figure 2.4: The domain used when performing standard CFD simulations

To simulate the car traveling along a road, the wheels are rotated and the complete ground is set as a moving ground boundary condition. To model the rotating wheel accurately is a difficult process in CFD and there exist different approaches. At Volvo Cars MRF zones are used which means that the fluid situated inside in between the rim spokes

are rotated along with the wall surfaces of the rims and tires which are not normal to the flow.

As the aerodynamic simulations at Volvo Cars are performed with moving ground and rotating wheels, care has to be taken concerning the tires deformation. In reality when a car is stationary the tires are deformed by the vehicle's own weight. When the wheels are rotating the centrifugal force acts on the tires and the tires experiences three different deformations in addition to the deformation caused by the car's weight. The three deformations are; radial expansion, axial contraction and vertical displacement.

To represent the deformation of the tires, a procedure at Volvo Cars is performed called morphing, which means that the surface mesh of the tires are deformed. The morphing procedure was created in a master thesis project performed by Peter Mlinaric [2] where also the use of MRF zones for modelling rotating wheel was studied.

3 Theory

In this chapter the theory behind the numerical simulations performed in this master thesis is briefly stated and explained. For more detailed information the reader is directed to the Fluent Theory Guide and to Ref. [4].

3.1 The Governing Equations

The flow of a Newtonian fluid is described by the governing equations consisting of the continuity equation and the Navier Stokes equations. For automotive industry calculations the velocity of the flow is never any higher than 250 km/h and therefore the flow can be considered to be incompressible. The incompressible continuity and Navier Stokes equations is displayed below by equation 3.1 and equation 3.2.

$$\frac{\partial v_i}{\partial x_i} = 0 \quad (3.1)$$

$$\rho \frac{\partial v_i}{\partial t} + \rho \frac{\partial v_i \partial v_j}{\partial x_j} = -\frac{\partial p}{\partial x_i} + \mu \frac{\partial^2 v_i}{\partial x_j \partial x_j} \quad (3.2)$$

To solve the equations, a solver uses different numerical schemes. In Fluent several different numerical schemes are available, such as 1st-order upwind, 2nd-order upwind and QUICK with the last two being the most accurate but also less stable. There is also different interpolation schemes available for the pressure and at Volvo Cars the default standard pressure interpolation scheme is used. The standard scheme uses equation 3.3 where the pressure is interpolated at the faces using momentum equation coefficients.

$$P_f = \frac{\frac{P_{c_0}}{a_{p,c_0}} + \frac{P_{c_1}}{a_{p,c_1}}}{\frac{1}{a_{p,c_0}} + \frac{1}{a_{p,c_1}}} \quad (3.3)$$

3.2 The Near Wall Flow

A turbulent flow is greatly affected by the walls as they are the main source of mean vorticity and turbulence. It is near the walls where the gradients are large and thus where the momentum is most affected. It is therefore of high importance in numerical simulations to accurately predict the near-wall flow.

A turbulent boundary layer consist of different layers with different characteristics. Immediately near the wall there is a very thin viscous sub-layer, followed by the buffer layer and then the log-law layer. To be able to resolve a complete turbulent boundary layer and account for the viscous force in the viscous sub-layer, a very fine mesh would be needed. Since this is not feasible with today's computer capacity, wall functions are instead employed to represent the effect of the wall. Normally wall function are used depending of the value of the variable y^+ , shown in equation 3.4. y^+ is the dimensionless distance to the wall for the cell closest to the wall and generally the wall functions are valid when y^+ is between 30 and 500, the range of the log-law layer.

$$y^+ = \frac{\rho u_T y}{\mu} \quad (3.4)$$

In Fluent however, a different variable, y^* , is used instead of y^+ . y^* is displayed in equation 3.5 and is approximately equal to y^+ in equilibrium turbulent boundary layers. Fluent employs the standard wall function when $y^* > 11.225$. If $y^* < 11.225$ the flow is considered to be laminar and a laminar stress-strain relationship is employed. This means that it is very important to keep y^* above 11.225 in areas where high turbulence and velocity is expected. The ideal would be to have y^* close to but above 30 in such areas.

$$y^* = \frac{\rho C_{\mu}^{(1/4)} k^{(1/2)} y}{\mu} \quad (3.5)$$

4 Method

This section describes the process performed in this master thesis in order to obtain the forthcoming results. There were three different main cases simulated, namely; Empty PVT tunnel, PVT tunnel with a simplified S60 and PVT tunnel with a detailed S80. The S80 was performed with two different configurations, closed front where only the external flow is simulated and open cooling where also the flow through the engine bay and cooling package is included. To be able to compare the results of the PVT tunnel simulations with the standard procedure at Volvo Cars, simulations according to computational procedures AEDCAE01 [5] and AEDCAE02 [6] were performed with the S60 and S80 model. The standard simulation is referred to as CFD tunnel and the PVT simulation as PVT tunnel through out this report.

4.1 Geometry

4.1.1 PVT Tunnel

To be able to keep the amount of cells within a reasonable level and due to the limited CAD available, only the nozzle, test section and diffuser of the wind tunnel were modeled. This means that some of the characteristics of the wind tunnel were lost, as the effect of the 90 degree turns before and after the test section on the flow field was not accounted for. Also, to ensure to get a stable solution, the domain was extended in the x-direction in three 10 meters long rectangular boxes. The idea was to remove these extensions one by one to see if their absence affected the solution negatively but since they only slightly increased the cell count they were never removed. The outer surface of the wind tunnel can be seen in Figure 4.1, the yellow part being the extension.

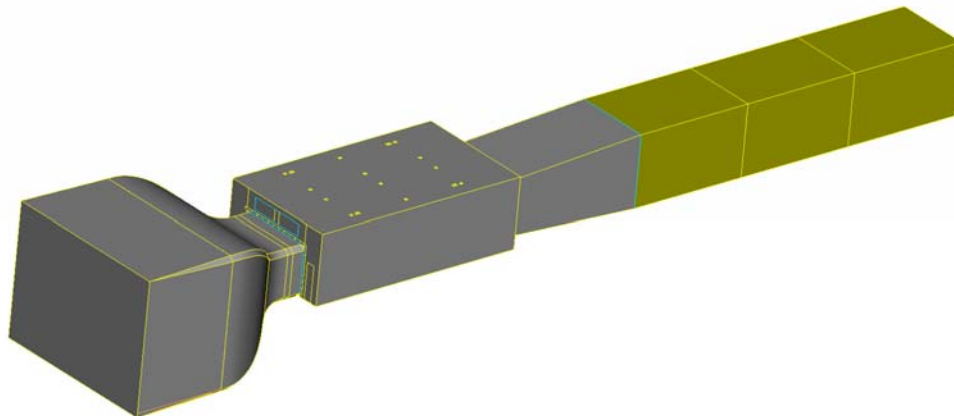


Figure 4.1: The outer domain of the wind tunnel

Figure 4.2 and Figure 4.3 shows a zoom in on the slotted walls with the test section's outer walls and roof removed, for the left and right side respectively. Notice the difference in the support structure of the slotted walls, left side compared to right side.

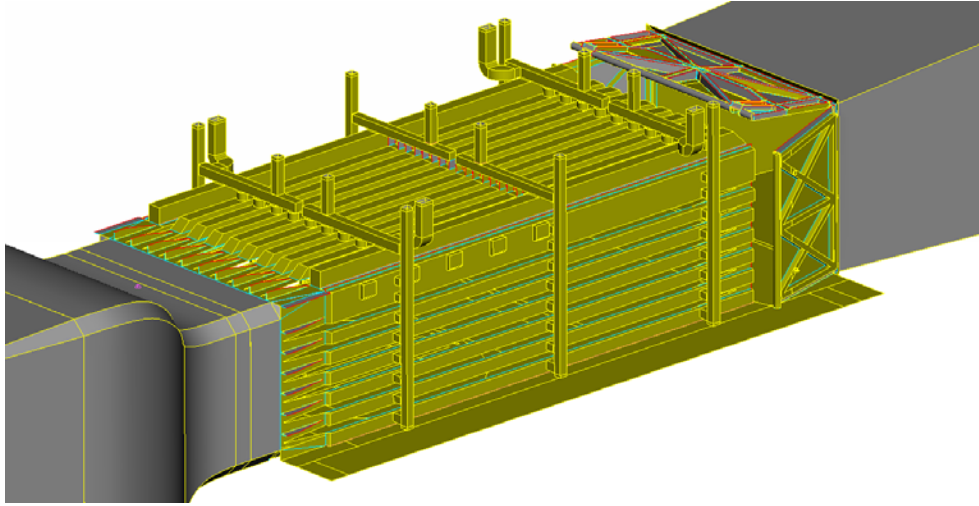


Figure 4.2: The domain of the test section with the test section's outer walls removed, left side

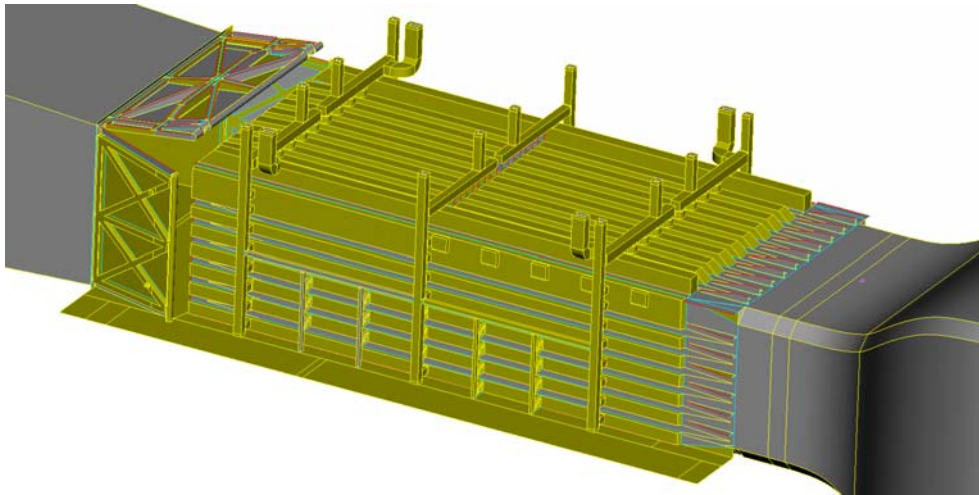


Figure 4.3: The domain of the test section with the test section's outer walls removed, right side

The domain was restricted by the available CAD geometry of the wind tunnel which only included the nozzle, diffuser and the main parts of the test section. Objects like cable ladders and air hoses were not part of this CAD and therefore not included. The CAD was also simplified, meaning that objects smaller than approximately 10 cm were removed. The biggest objects missing in the CAD was two overhead cranes, one situated above the slotted ceiling and the other one at the end of the diffuser. The first one was not believed to affect the flow significantly because of its position away from the free flow and rather small size and was therefore left out. The other crane's influence however could not be minimized that easily as its position was in the free flow, even though far from the test section. It was decided to proceed with the calculation without the cranes but if the results showed difference between the CFD and experiments which could be because of the absence of the cranes they would be created by hand and added to new simulations.

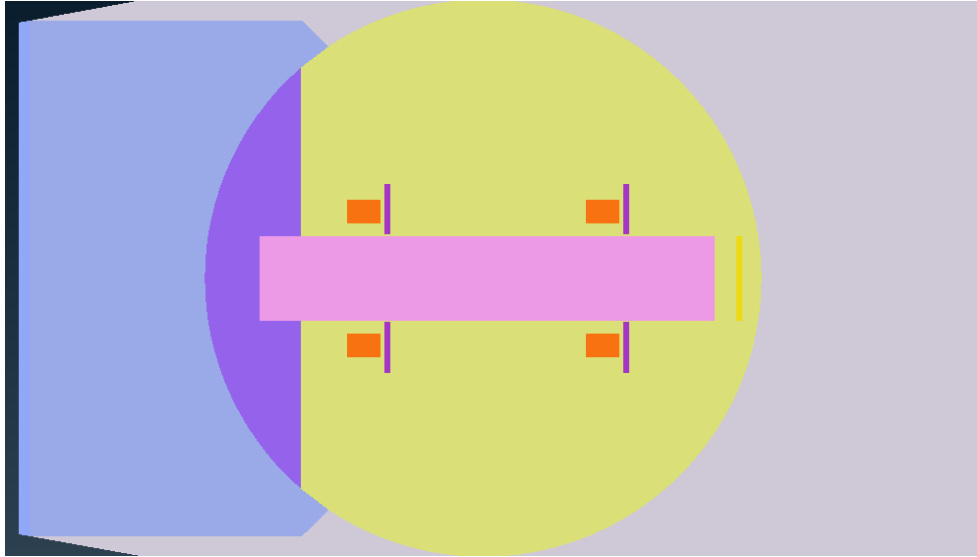


Figure 4.4: The geometry of the floor

The floor of the test section, which is shown in Figure 4.4, included the same main parts used for aerodynamic evaluations; turn table, center belt, WDUs, tangential blowing and the two suction zones. However, it was simplified to be completely flat, hence featuring no gaps around the center belt, no small holes pattern in the suction zones and no vertical inlet for the tangential blowing. These gaps and holes were considered too small to be included and were replaced with continuous surfaces and the tangential blowing's vertical inlet was replaced by the corresponding horizontal area where the incoming air would join the flow in the tunnel. The mesh resolution required in order to include all the details mentioned above would result in mesh sizes too large and impractical for the scope of this work.

4.1.2 S60

To be able to investigate the behaviour of the flow field with a car inside the tunnel without using too much time in the meshing and calculation process it was decided to start with a symmetric S60 with flat floor and solid wheels. Choosing a symmetric model would also remove any chance that the car would be the cause behind any asymmetrical behaviour of the flow.

The S60 model used was an Aeroacoustic model with a flat underbody. However, this meant that the exterior was more detailed around the a-pillars than a normal Aerodynamic model, while the wheels and underbody were much simplified. The exterior of the S60 is shown by Figure 4.5. Also, the S60 model incorporated a very steep diffuser, which can be seen in Figure 4.6.

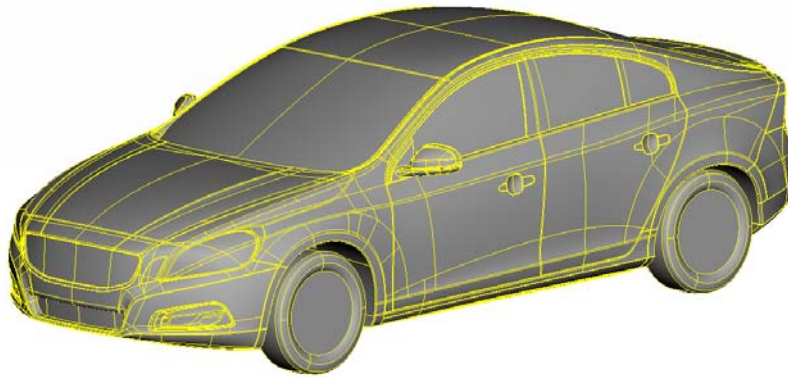


Figure 4.5: The S60 model

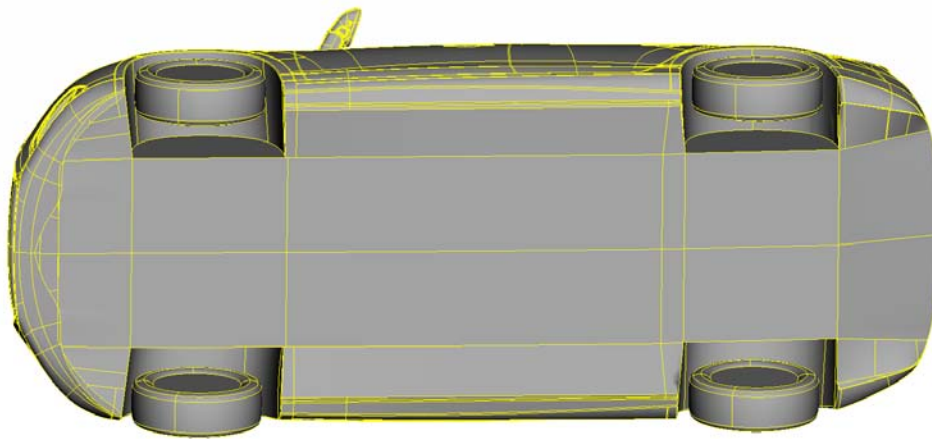


Figure 4.6: The flat floor of the S60 model

4.1.3 S80 Closed Front

As there exist a vast number of different variants of S80 models and only a few of them are converted from CAD to CFD, it was hard to find an exact copy of the 2007 S80 that was going to be used for the real experiments in the wind tunnel. Instead a S80 with a different configuration had to be modified by comparing the model with pictures of the 2007 S80. However, as this was a very time consuming process, some features at the underbody of the 2007 S80 could not be replicated. This was a compromise that had to be taken and will be a source of error in this master thesis. The S80 model is pictured in Figure 4.7 and 4.8.

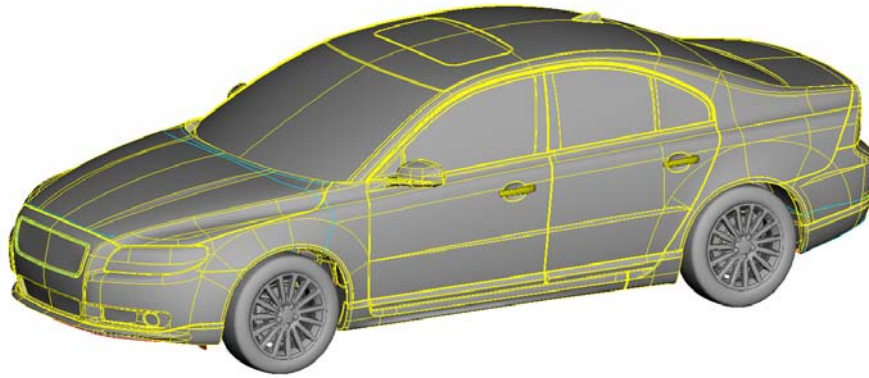


Figure 4.7: The S80 closed front model

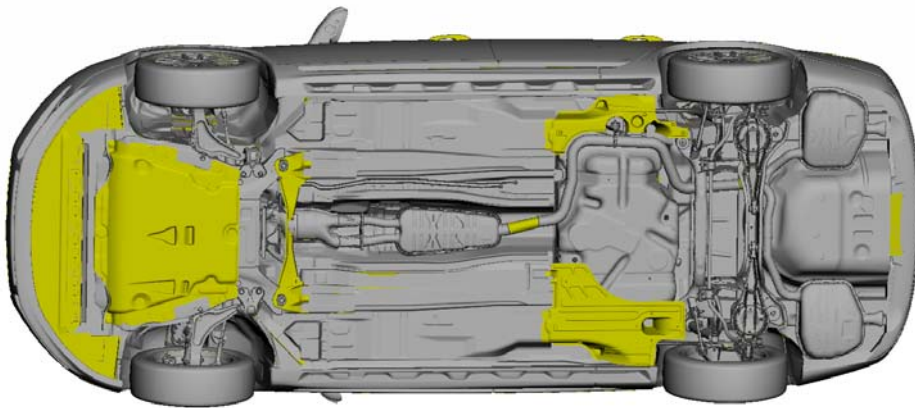


Figure 4.8: The floor of the S80 closed front model

To do a closed front simulation, the upper and lower grill was closed of by a flat surface in order to stop air from entering the engine bay. The engine bay was also sealed at the bottom by flat surfaces which effectively meant that no part of the engine bay would be used for the closed front simulation, all according to computational procedure AEDCAE01 [5].

4.1.4 S80 Open Cooling

In the Open Cooling case the grills were left open and the air was let through the cooling pack and engine bay area. The cooling pack consisted of the main fans and radiators in the same detail as standard open cooling simulations performed at Volvo Cars [6]. This is however more simple than a real production car which have even more objects and parts in the engine bay and cooling pack area. The geometry of the grill and part of the engine bay can be seen in Figure 4.9, where the left side of the exterior has been removed.

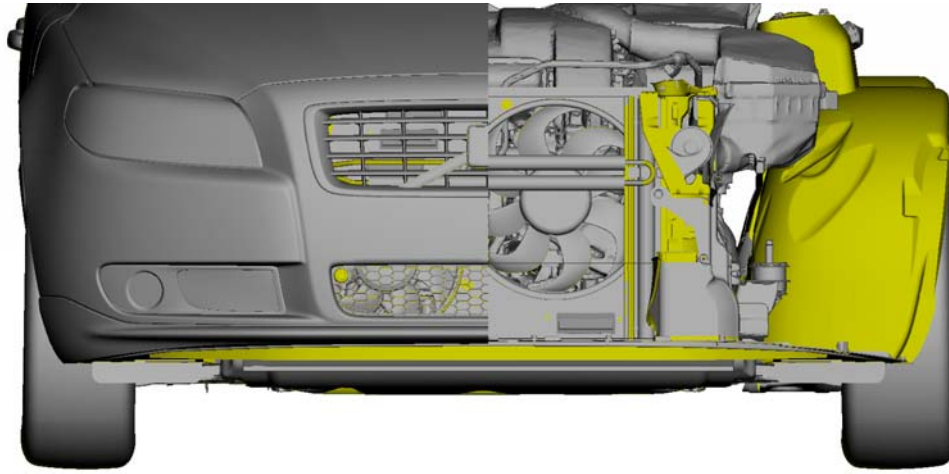


Figure 4.9: Front view of the S80 open cooling model

4.2 Mesh

4.2.1 PVT Tunnel

The volume mesh was created with Harpoon, with the maximum cell size set to 160 mm. To resolve the geometry as good as possible the smallest cell used was 5 mm. The mesh distribution of the symmetry plane can be seen in Figure 4.10.

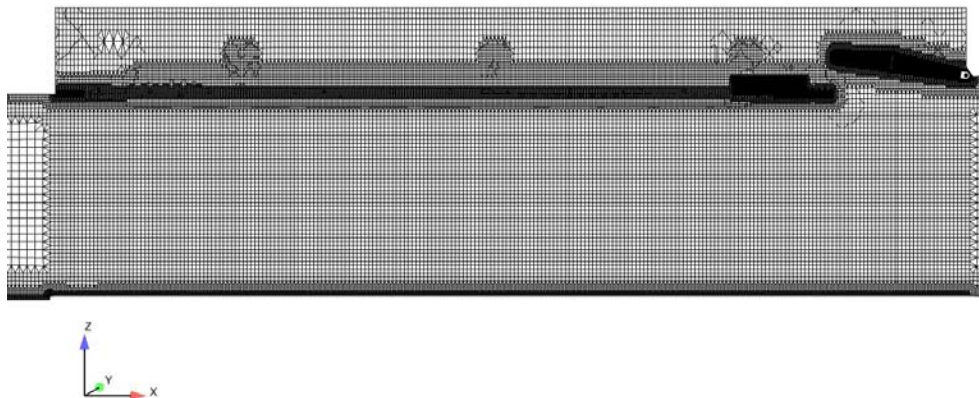


Figure 4.10: Mesh distribution of the symmetry plane

In order to keep y^+ between 30 and 500, three prism layers with a first layer height of 2 mm were added to the volume mesh. Since prism layers is hard to produce in Harpoon with good quality even for simple geometries, they were restricted to the area around the test section, hence to the slotted walls, diffuser, floor and part of the nozzle closest to the test section. In an optimal case, the prism layer height would have been varied depending of the velocity at the walls in order to always keep y^+ close to 30. However, this was not possible to do in Harpoon in a simple way and instead an approximated height of 2 mm was chosen. A height of 1 mm had been tested but produced y^+ values well below 30 in

some areas, which was not adequate. The resulting y -plus of the walls is presented by Figure 4.11. Where there are prism layers y^+ is approximately between 30 and 150.

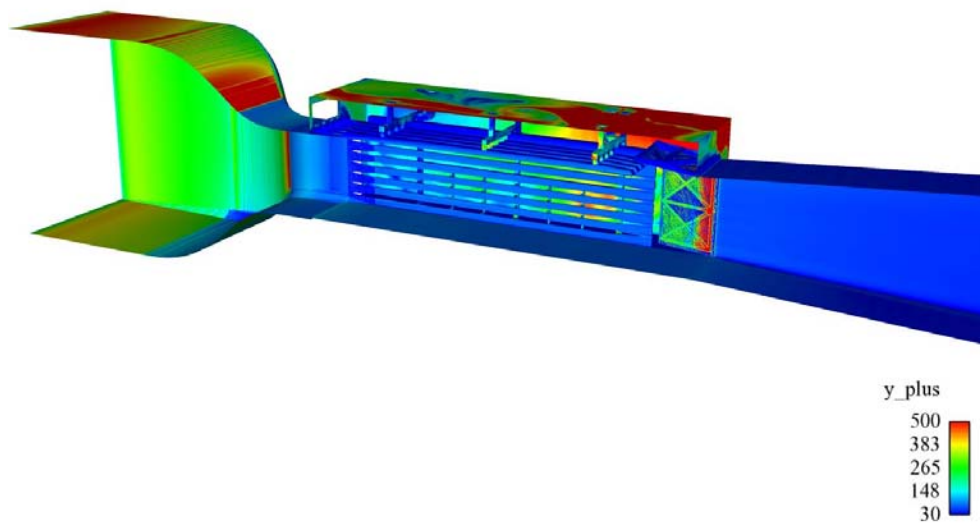


Figure 4.11: y^+ on the walls of the tunnel

When creating the prism layers, care had to be taken to the area around the nozzle, due to the accelerating flow and thus increasing friction velocity. When looking at some early simulation results there were no distinctive line where the prism layers were needed, therefore the prism layers creation was started at an approximated position at the center of the nozzle. This was a compromise but the easiest and quickest way of producing fairly accurate results.

In the beginning the surface cell sizes were only small enough to resolve the geometry but convergence problems which was believed to be mesh related forced the surface cell sizes to be decreased and refinement zones to be added. A large refinement box where added which enclosed the whole test section within the slotted walls and small boxes where added at the rear of the slotted walls, in between the slots. The resulting number of cells for the empty tunnel ended at 78 million. In the end the convergence problems showed not to be due to a too coarse mesh but because of wrongly defined boundary conditions. The fine resolution was kept anyway as the number of cells was still below a plausible level.

4.2.2 S60

When setting up the meshing settings for the S60 , the normal procedure at Volvo Cars for an aerodynamic simulation was followed [5]. It was important that the cell sizes of the car surfaces and the density boxes around the car was essential the same as the normal case performed at Volvo Cars. The resulting surface cell sizes of the car ranged from 5 mm down to 1.25 mm. The mesh quality and the surrounding refinement boxes is displayed in Figure 4.12.

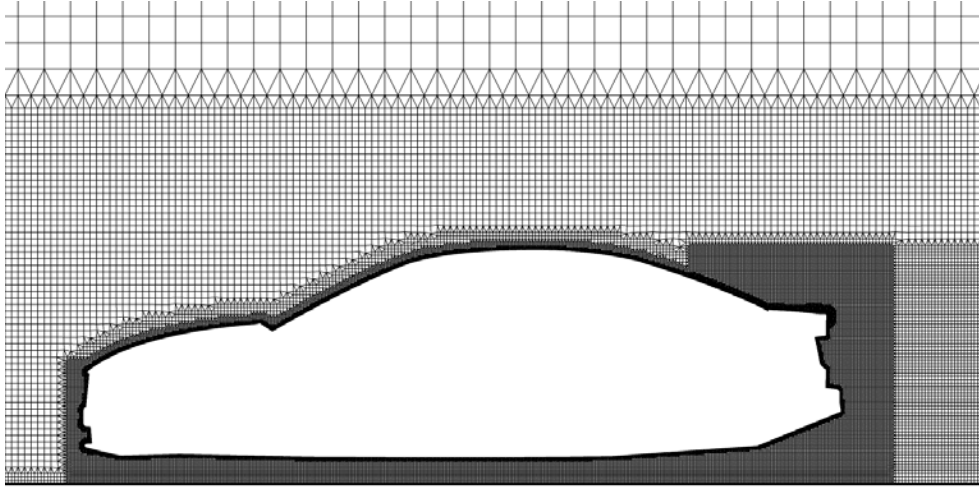


Figure 4.12: Mesh distribution across the symmetry plane of the S60

As no prism layers is used, y^+ becomes sensitive to the level of refinement needed to resolve the car geometry. This can be seen in Figure 4.13 where the lowest values y^+ is found at refined areas such as the rear of the car and the a-posts. Mostly, y^+ is around 250 and never goes lower than the laminar limit which correspond to a y^* value of 11.225. Figure 4.13 also shows another consequence of having no prism layers as the mesh method applied by Harpoon creates fictitious oval patterns across the surface of the car.

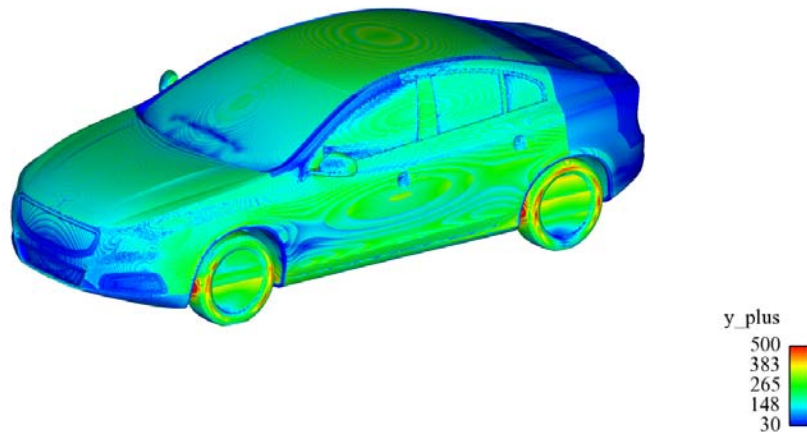


Figure 4.13: y^+ on the S60

In order to keep the amount of cells down to a acceptable level, the surface cell sizes of the PVT tunnel was decreased without compromising the resolution of the geometry. This meant that the number of cells for the tunnel with the S60 was kept at 65 million instead of being well above 100 million.

4.2.3 S80 Closed Front

The volume mesh for the S80 was created with the same PID distribution, surface cell sizes and refinement boxes which had been used in previous simulations of the S80, the same approach as for the S60 [5]. This meant that four refinement boxes was added, where one

large refinement box covered the whole car, one enclosed the area under the car and the two other was placed at the rear and the wake of the car. The cell distribution around the car and across the symmetry plane is showed in Figure 4.14. The detailed floor increased the cell count heavily resulting in a volume mesh of 76 million cells.

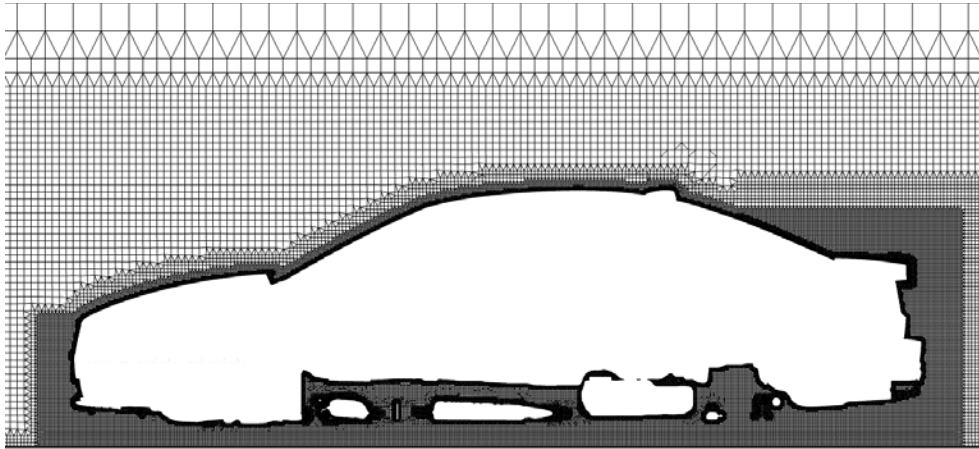


Figure 4.14: Mesh distribution across the symmetry plane of the S80 closed front

The surface cell sizes ranged from 5 mm to 1.25 mm, a resolution which resulted in the y^+ distribution showed in Figure 4.15. Just as for the S60, y^+ is sensitive to the degree of refinement and the same fictitious oval patterns are created on the surface of the S80.

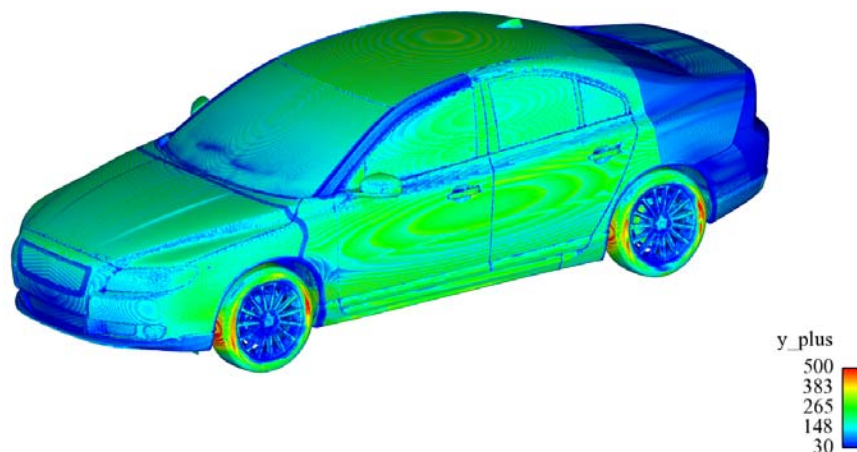


Figure 4.15: y^+ on the S80

4.2.4 S80 Open Cooling

Since also the fully detailed grill, spoiler opening and engine bay area were included in the S80 open cooling model, the cell count inevitably became a lot higher compared to the closed front model due to the small cell size needed to resolve the complicated geometry and the total cell count ended at 114 million cells. The symmetry plane of the engine bay area of the S80 is shown in Figure 4.16 and a refinement box around the cooling package

is visible as the more black and dense area. However, this refinement box was omitted by mistake in the PVT simulation and was only included in the simulation of the CFD tunnel.

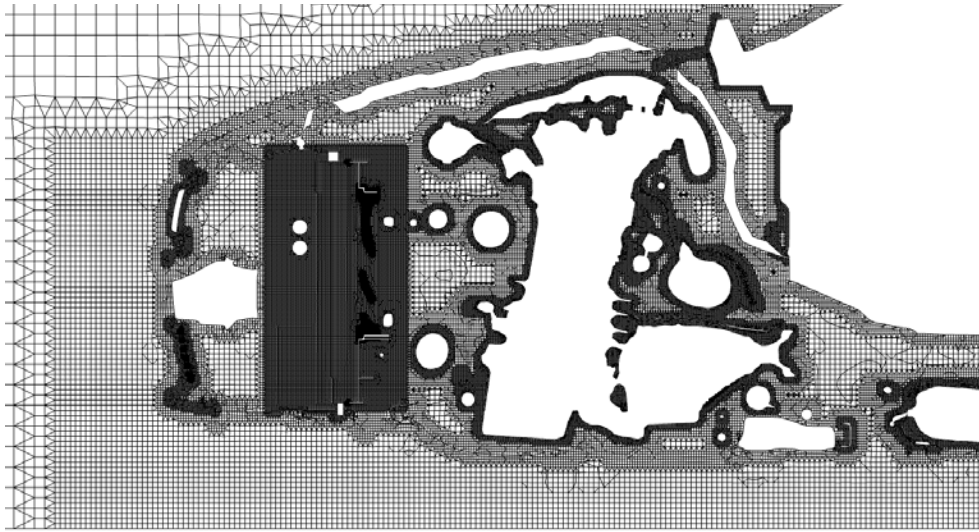


Figure 4.16: Mesh distribution across the symmetry plane of the S80 engine bay

As the S80 open cooling had the same level of refinement of the exterior as the closed front version, it had also the same y^+ distribution across the surface, thus no new figure is needed here, instead see Figure 4.15.

4.3 Calculation Settings

In the PVT tunnel the velocity is calculated from the pressure difference(dp) in the nozzle, measured by the two pressure taps P_{C1} and P_{C2} . P_{C1} is located just before the contraction of the nozzle and P_{C2} is located after the contraction, before the test section, as shown by Figure 4.17.

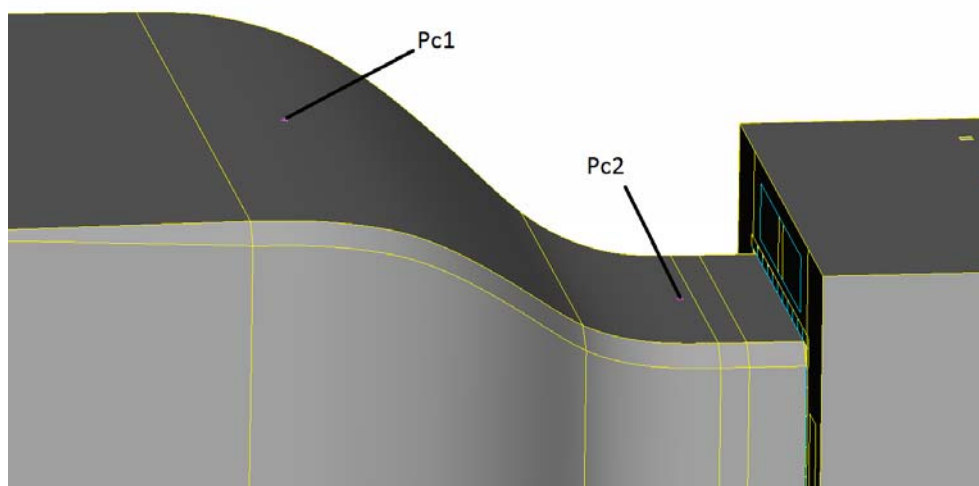


Figure 4.17: Locations of P_{C1} and P_{C2} on the nozzle roof

In the figure, the pressure taps are located at the centre line of the nozzle but in reality there are two pressure taps on each side of the centre line and the pressure is taken as the average between these two positions. However, results showed that the pressure did not

vary in any significant magnitude in the y direction and only one position at the centre line was used for most of the simulations. From dp , P_{C1} and P_{C2} the calibration coefficients k_p and k_q are calculated through equations 4.1 and 4.2, where P_s and P_t is the static and total pressure at the position where the desired velocity is calibrated.

$$k_p = \frac{P_s - P_{C2}}{P_{C1} - P_{C2}} \quad (4.1)$$

$$k_q = \frac{P_t - P_s}{P_{C1} - P_{C2}} \quad (4.2)$$

When the tunnel was calibrated by Aiolos [7], a pitot tube was placed in center of the turntable measuring the static and dynamic pressure, 1.2 meters above the floor, making it possible to calculate the calibration coefficients for different velocities. This gave a correlation between dp in the nozzle and the velocity in the test section for each different configuration of the tunnel. The resulting polynomial coefficients for the equation $b*dp+a$ which is used to calculate the calibration coefficients for each configuration is shown in the tables below.

Table 4.1: The calibration coefficients for Scoop only mode

Coefficient	a	b
k_p	0.047052534	-0.000002348
k_q	0.971833432	0.000003161

Table 4.2: The calibration coefficients for GESS off mode

Coefficient	a	b
k_p	0.060246216	-0.000002456
k_q	0.958619998	0.000003841

Table 4.3: The calibration coefficients for Aerodynamic mode

Coefficient	a	b
k_p	0.063270435	-0.000004086
k_q	0.958670736	0.000003667

When a car is inside the tunnel it is impossible to measure the velocity at the center of the turn table as that is where the car is positioned. Instead the velocity is calculated by using the calibration coefficients and the pressures measured at the contraction taps, P_{C1} and P_{C2} . In order to achieve a certain velocity in the test section with a car inside, dp is set to the same dp which produced the sought velocity in an empty tunnel.

However, since the CFD-simulation produced different dp than the real PVT, the real calibration coefficients could not be used in the CFD as they gave an incorrect velocity in the test section. Also, when performing half tunnel calculations for different velocities, the real calibration coefficient was found to produce incorrect C_p plots. In Figure 4.18, C_p , calculated with Aiolos calibration coefficients, is plotted for four different velocities along the center line of the test section at a height of 600 mm. The calibration coefficients merely translates the C_p upwards for decreasing velocity and does not counteract the decrease in

dp which comes with decreasing velocity as they should. Note that C_p is displayed as C_{p_64} in these figures which equation is stated in the Postprocessing chapter.

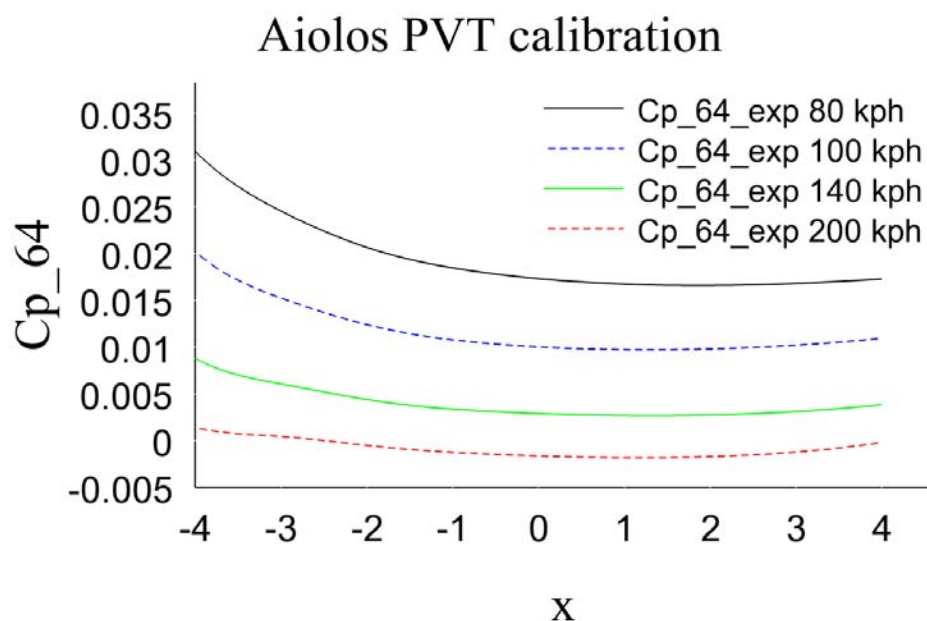


Figure 4.18: C_p calculated with the real calibration coefficients along the center line with Scoop only mode

Instead new calibration coefficients were calculated with equations 4.1 and 4.2 for the empty tunnel and the same values were used for simulations with a car. For this method to be completely accurate the dp had to be the same for both the empty tunnel and the tunnel with a car as the calibration coefficients were dependent on dp . The resulting C_p across the center line in an empty tunnel can be found in Figure 4.19. The new calibration coefficients predicts a correct test section velocity and accounts for the varying dp , proved by the fact that the C_p of different velocity cross at the same position, $x=0.4m$.

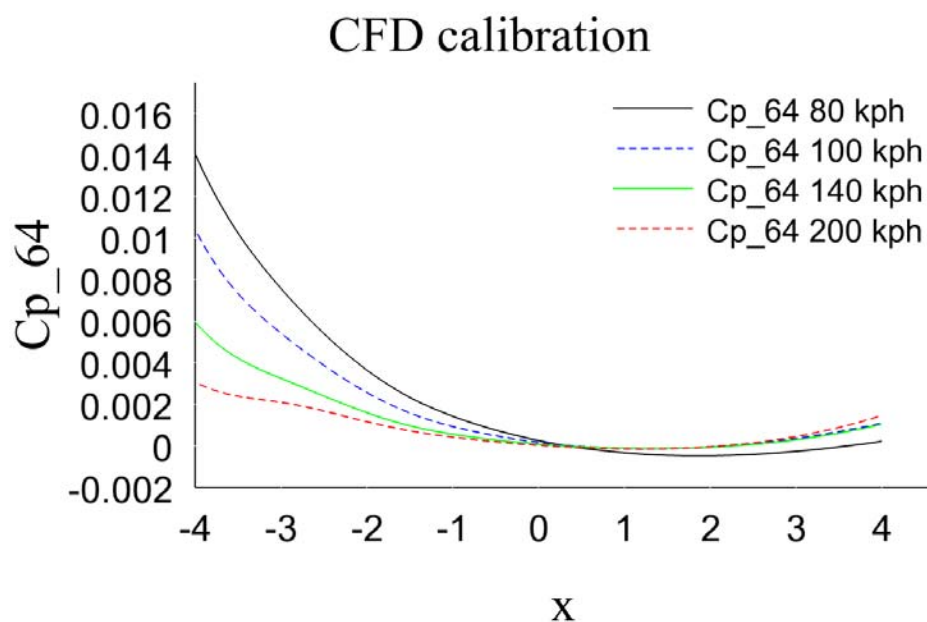


Figure 4.19: C_p calculated with the new calibration coefficients along the center line with Scoop only mode

4.3.1 Empty Tunnel

For the CFD calculations the settings was set to the same as is used for regular aerodynamic calculations at Volvo Cars to be able to compare the results. This meant that the simulations were restricted to the realizable k-epsilon turbulence model with default coefficients and 2nd order upwind schemes was only used for the momentum, while 1st order upwind schemes was used for the turbulent kinetic energy and the turbulent dissipation rate.

Three different configurations were simulated, Scoop only, GESS off and Aerodynamic mode. Scoop only refers to the case when only the basic suction scoop is activated, hence 1st/2nd suction, tangential blowing, center band and WDU's are all turned off. GESS off means that the ground simulation system is deactivated and only the basic suction scoop and 1st and 2nd suction is turned on. In the third configuration, Aerodynamic mode, the complete boundary control system is activated.

When a device of the BLCS was used in the simulation, the boundary condition was changed from wall to mass flow inlet. A positive or negative vector was set depending on if the device would suck air out of the system or blow air into the system. The mass flow values set were interpolated from the max flow rate data collected from the report "Upgrade of the Volvo Cars Aerodynamic Wind Tunnel" [1] for each test section velocity simulated. However, cubic meter per second values was mistakenly applied instead of mass flow rate values, a mistake that meant that the mass flow values were 20 % lower than in reality.

To be able to model the tangential blowing, which in reality were just a thin column on the floor, a horizontal surface were created corresponding to the horizontal cross section of the tangential blowing inlet. A vector calculated from the slope of the surface after the tangential blowing column was then defined. This vector had a x-coordinate almost 68 times larger than the z-coordinate, making it almost completely aligned with the floor.

As the type of configuration affects the whole velocity field, all the configurations had to be calibrated for a velocity of 140 kph(38.889 m/s) in the test section. The velocity was measured at a point 1.2 m above the center of the turn table, the same position as the Prantl tube used for calibrating the physical wind tunnel. Since the geometry featured a convergent nozzle the inlet velocity would be a lot lower than the velocity in the test section and to find the correct inlet velocity the law of conservation of mass was first used to calculate an approximated inlet velocity. In order to distinguished the test section velocity's dependency on dp , four different test section velocities were simulated; 80 kph, 100 kph, 140 kph and 200 kph. The inlet velocities was in each case approximated with mass conservation. The simulations was done on a half tunnel with Scoop only mode and the results showed that the test section velocity was linearly dependent on dp . This meant that the correct inlet velocity could accurately be interpolated with the use of dp and the desired test section velocity for each configuration.

4.3.2 Tunnel With Simple S60

Simulations with a car in the tunnel was only performed with the configuration Aerodynamic mode as it was the most common configuration used for experiments. The inlet velocity for the PVT tunnel with a S60 was interpolated to a velocity that gave the same pressure difference as an empty tunnel with Aerodynamic mode. Later it was discovered that the pressure difference used was not corresponding to a velocity of 140 kph in the test section but slightly lower. Since the goal with the simple S60 was not to compare with real life experiments but to investigate the asymmetric behaviour of the flow inside the PVT tunnel, no new simulations was performed.

4.3.3 Tunnel With S80 Closed Front

The S80 was at first only simulated with Aerodynamic mode, but a simulation with the tangential blowing turned off was later also performed. This was done by simply changing the boundary condition of the tangential blowing from inlet mass flow to wall. The velocity at the inlet was interpolated in the same way as for the S60 to give the same pressure difference across the nozzle as the empty tunnel.

To accurately simulate the rotation of the real rims which the S80 model incorporated, MRF zones was used, which meant that the fluid in between the spokes was rotated along with the surfaces of the rim which were tangential to the flow direction, according to computational procedure AEDCAE01 [5].

4.3.4 Tunnel With S80 Open Cooling

The inclusion of the cooling package in the S80 open cooling modelled meant that the pressure drop and the rotating fans had to be accounted for. The pressure drop was taken from measurements and simple specified in Fluent by the radiator boundary condition. The movement of the two fans was modelled in almost the same way as the rotating wheels, thus with MRF zones, difference being that the complete zone enclosing the fan was rotated and not just only the fluid in between the fan blades.

4.4 Postprocessing

When comparing CFD results with experimental results it is very important that the variables are normalized in the same way in both CFD and the experiments. Normally C_p is calculated using a free stream static pressure and the free stream dynamic pressure according to equation 4.3.

$$C_p = \frac{P - P_{s,ref}}{q_{ref}} \quad (4.3)$$

But since the reference pressures is hard to define in the PVT tunnel C_p have to be calculated in a different way. Instead of the standard definition, C_p was calculated with the use of the calibration coefficients together with dp and P_{C2} . The PVT C_p equation is displayed in equation 4.4 and this C_p equation is referred to Cp.64 in figures and graphs throughout this report.

$$C_p = \frac{P - P_{C2}}{(P_{C1} - P_{C2}) * k_q} - \frac{k_p}{k_q} \quad (4.4)$$

To be able to compare the dynamic pressure uniformity in an empty tunnel with experiments performed by Aiolos, the dynamic pressure was calculated in the same way as in the experiments. The equation used by Aiolos is shown by equation 4.5, where $k=1.4$. As the pressures needed to be in absolute values, the reference pressure of 101325 Pa used in the CFD was added to the static values. The dynamic pressure was then normalized in the CFD by the free stream dynamic pressure taken at the center of the turn table at $z=1.2$ m. This was somewhat different than in the experiments where the facility evaluated test section dynamic pressure was used.

$$q = \frac{k}{k-1} * P_s * \left(\frac{P_t - P_s}{P_s} \right)^{k-1/k} - 1 \quad (4.5)$$

During James C. Lyon's master thesis [8], where wind tunnel experiments were compared with coast down tests on the open road through pressure taps on the center line of the car, a different way of calculating C_p was used where the reference pressures were taken at the hood of the car, close to the windscreen, and in front of the car. The same definition of C_p was therefore applied on the CFD results in order to be able to compare them with the results from James C. Lyon's experiments. Despite using the same stated positions for the reference pressures as described, the result showed to be very different and not completely believable so instead the PVT definition, equation 4.4 was used for the CFD results. Also, the exact positions of the pressure taps used during the experiments was not known and instead they were arbitrary placed by looking at the center line pressure plots of the experiments. Due to large gradients in certain areas of the car, a slight change in the position of a pressure point could change C_p considerably. This will have to be kept in mind when analyzing this comparison in the result section.

5 Results and Discussion

The results in this chapter are presented in the same order as in chapter 4, Method; first empty tunnel, then tunnel with S60 and last tunnel with S80.

5.1 Empty Tunnel

5.1.1 Asymmetrical Behaviour

In the beginning of this master thesis it was important to control if it was possible to only do calculations on one half of the tunnel, thus saving simulation time. However, it was quickly understood that the geometry of the PVT tunnel was far too asymmetrical and only simulating one half would not be sufficient due to the loss of information.

A good way to show that the asymmetrical slotted walls support have a big effect on the flow field is by plotting the pressure on the slotted walls. In Figure 5.1 the contour of the pressure is plotted on the right side of the slotted walls for Aerodynamic mode. Notice that the pressure drops at the smaller support beams and at the middle large beam. The scale is however very small, only a few pascals. The left side is shown in Figure 5.2 and the difference is quite significant. Here there are no small pressure drops as the smaller support beams are absent.

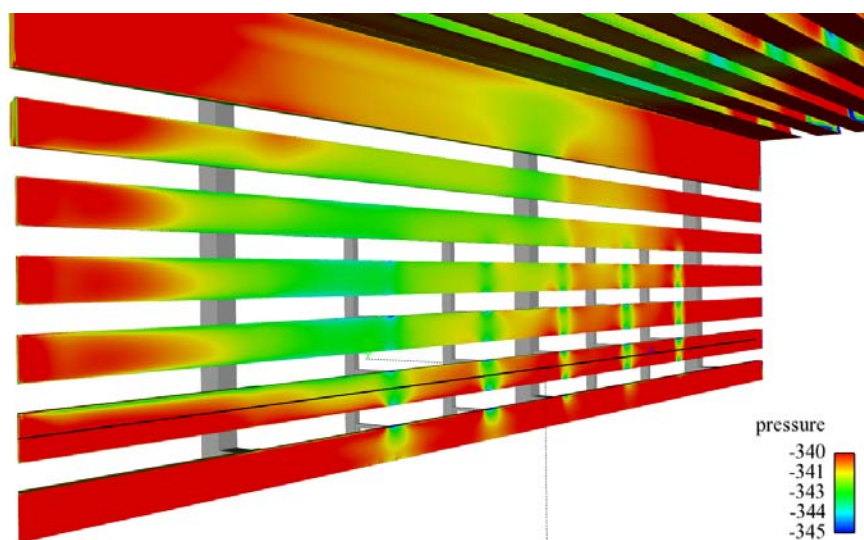


Figure 5.1: Pressure at the right wall in an empty tunnel with Aerodynamic mode

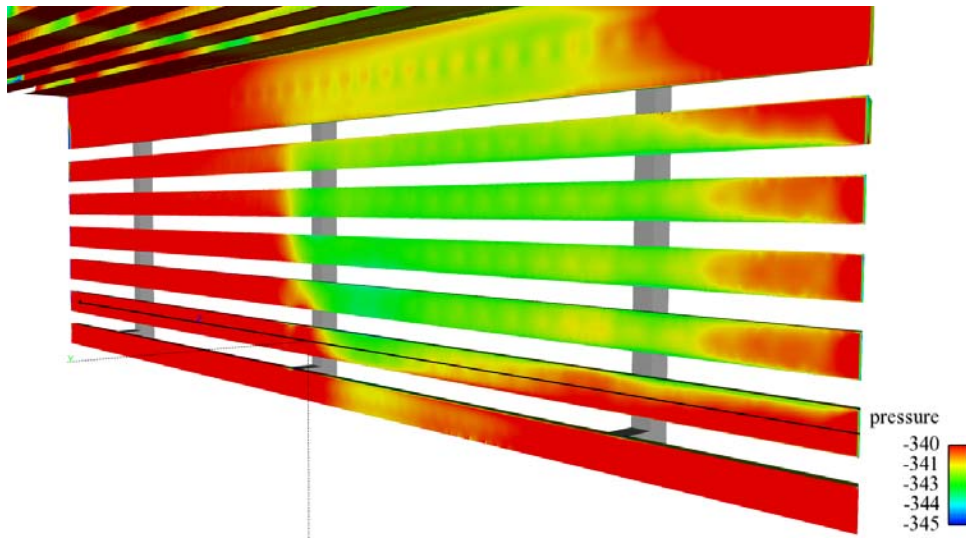


Figure 5.2: Pressure at the left wall in an empty tunnel with Aerodynamic mode

The asymmetry is even more evident when plotting C_p across one of the horizontal beams as shown in Figure 5.3. Usually when experiments is made and the aim is to examine the pressure on the slotted walls, pressure taps is placed on the 2nd horizontal beam element from the floor. To be able to compare the CFD with the experiments the same beam element was used. The black line in Figure 5.1 and 5.2 represents the line which C_p is plotted along in the following figures.

As can be seen by Figure 5.3, the difference between the right wall and left wall is pretty obvious. The four additional vertical support beams on the right side have a large impact on the flow inside the slotted wall. Instead of being smooth as on the left side, the curve is disturbed by the support beams and the pressure drops at each beam.

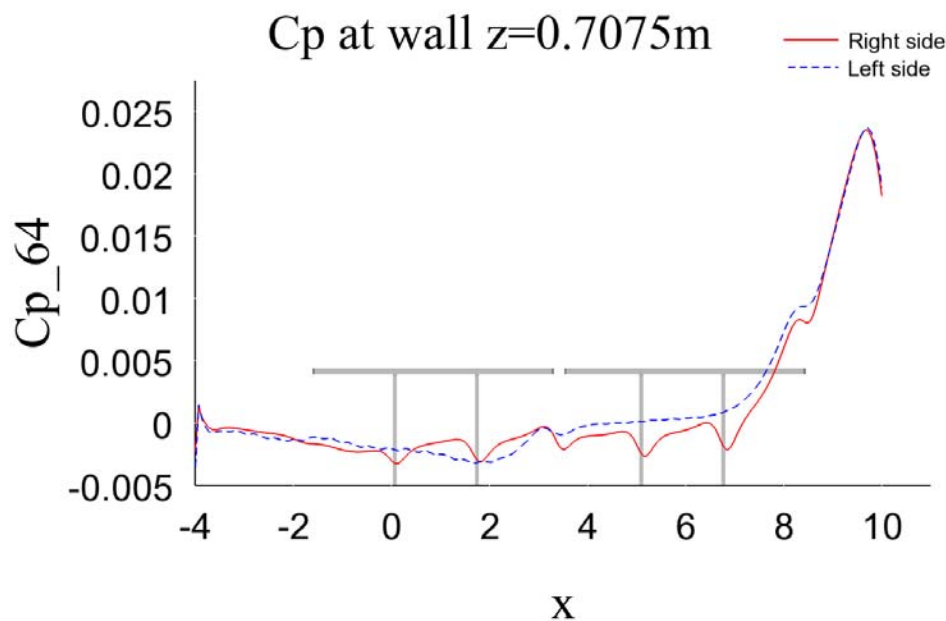


Figure 5.3: C_p at the wall in an empty tunnel with Aerodynamic mode

The four additional support beams is however not the only difference between the right and left side. As can be noticed in Figure 5.3 there is also a pressure drop between the pair of support beams where the drop is bigger on the right wall compare to the left wall. This is because the main vertical support beam which is found on both sides is different

on the right side. On the right side it has the same triangulated elements connecting it to the slotted walls as the additional support beams have which are different from the solid squared ones on the left side. The asymmetrical behaviour in the wind tunnel will be further investigated with a car inside the tunnel later in this report.

5.1.2 Axial pressure gradient

It is a known fact that when the PVT tunnel is empty, it has a positive axial pressure gradient across the test section. A positive axial pressure gradient means that the pressure is higher at the area where a car's front normally is situated compared to the area where a car's rear and wake is placed. This will affect the pressure distribution on a car in the tunnel in a way which increases the measured drag. Figure 5.4 shows C_p along the center line for four different heights and for Aerodynamic mode. It is clear from the figure that the PVT tunnel has positive axial pressure gradient.

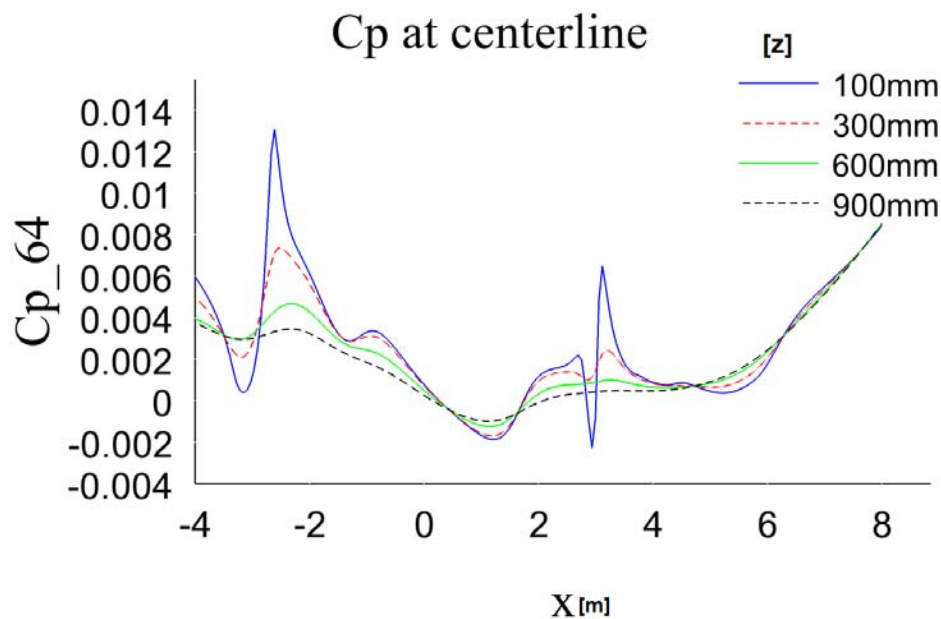


Figure 5.4: The axial pressure gradient across the center line for Aerodynamic mode

5.1.3 Nozzle Contraction

As P_{C1} and P_{C2} have a large impact on the way C_p is calculated, the pressure drop of the nozzle was examined. In Figure 5.5 the static pressure along the centerline of the roof of the nozzle for Scoop only mode is plotted. One would expect the pressure to drop consistently as the nozzle contracts and then at the end smoothly even out to a constant motion, but this is obviously not the case here. Instead the pressure curve reach its minimum at $x=-7.8m$ and then start to rise again before it rather chaotic assumes a constant behaviour. Evidently the flow separates here and the velocity decreases after the pressure minimum instead of continue to increase or become constant. The geometry of the nozzle does not seem to be as good as required to keep a good flow through the nozzle.

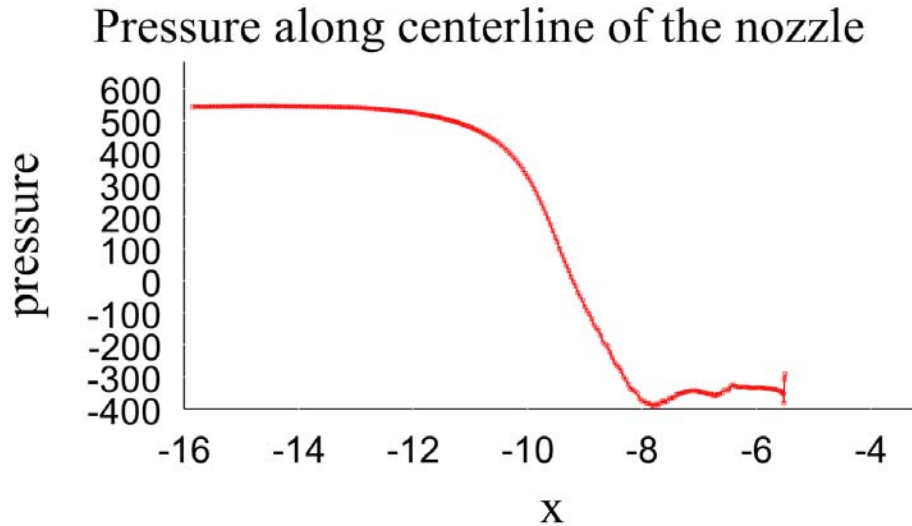


Figure 5.5: Pressure at nozzle roof with Scoop only mode

Since P_{C2} is positioned at $x=-7.25$, which is not where the pressure reaches its minimum, the pressure difference between P_{C1} and P_{C2} will not be equal to the true pressure difference over the nozzle. Also, if a steady simulation produces a curve like this, then it is possible that the pressure at P_{C2} in the real tunnel can have a non desired time dependent fluctuating behaviour.

To show that this results was due a non optimal geometry and not because of any CFD related error, for example a bad mesh, a new nozzle was designed which had a longer contraction than the original. To simplify the simulation and remove any impact of other objects in the tunnel like the suction scoop, the tunnel was turned into a solid walls tunnel. The difference between the original nozzle and the new nozzle can be seen in Figure 5.6 where the static pressure along the roof is plotted.

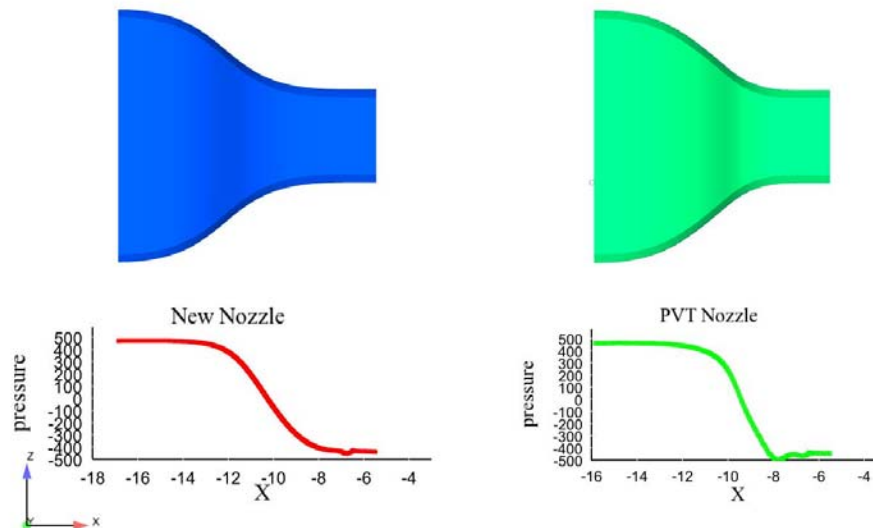


Figure 5.6: Pressure at nozzle roof

The new nozzle have a much smoother pressure curve because of the more forgiving contraction. The small bump experienced by both nozzles is situated where the surface

becomes horizontal. Refinements of the mesh at this area did not smoothen out the bump and therefore it can be concluded that it is not mesh related. Regardless, there is no doubt that the new nozzle would be a better solution than the original as the pressure drop is more consistent.

5.1.4 Comparison With Experiments

When comparing the CFD results with real experiments in the tunnel a big difference can be noticed, namely the magnitude of the pressure differences in the domain. In the CFD the pressure differences is a lot smaller than in the experiment. For example, C_p along the 2nd beam element fluctuates at the support beams with a magnitude of 0.002 in the CFD. In the experiments the magnitude of the fluctuations is a lot higher, more than 0.05. The big difference can be seen in Figure 5.7 and in comparison the CFD curve becomes almost like a straight line.

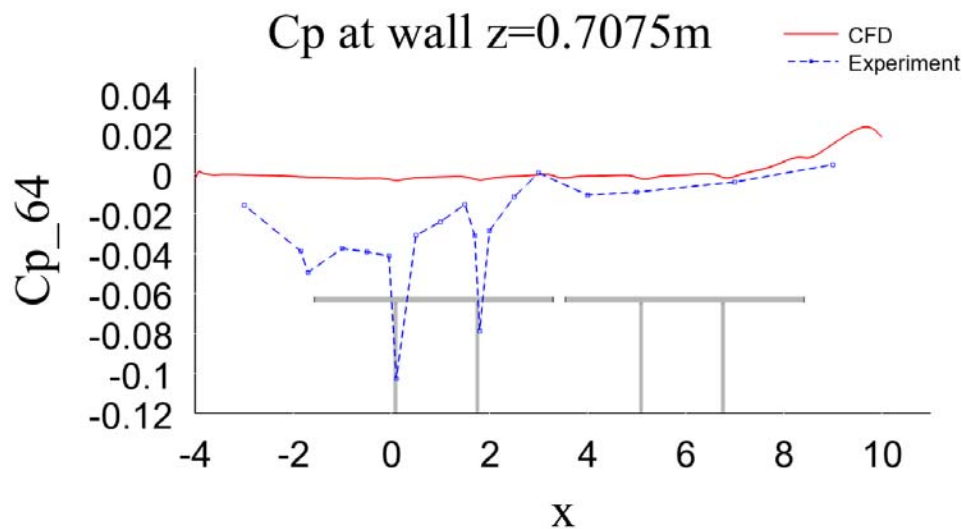


Figure 5.7: C_p at wall in an empty tunnel

Such a large difference was not expected and the reason behind it is not so easily explained. The flow in the PVT tunnel is natural unsteady and enforcing a natural unsteady flow field to give a steady solution as in the CFD simulation means that information is lost mainly due to time-averaging, but also because of the solver's habit of suppressing unsteady behaviour in order to produce better convergence. But the experiments is time-averaged as well which means that other factors must be behind the difference.

Another factor which effects the results is the uniformity of the flow. Figure 5.8 and 5.9 compares the normalized dynamic pressure from the CFD simulation with the measurements made by Aiolos [7], both with Aerodynamic mode, in two planes at x-position -2500mm and x-position 2500mm. The flow in the CFD simulation is a lot more uniform than in the experiment which could be the reason why the pressure felt by the slotted walls is of less varying degree.

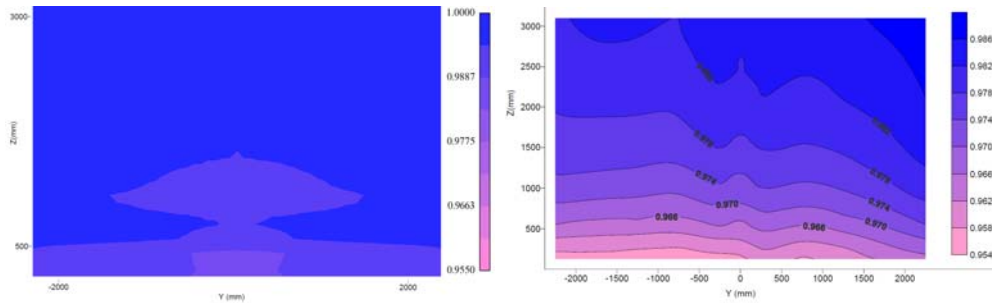


Figure 5.8: Dynamic pressure uniformity at $x=-2500$ mm

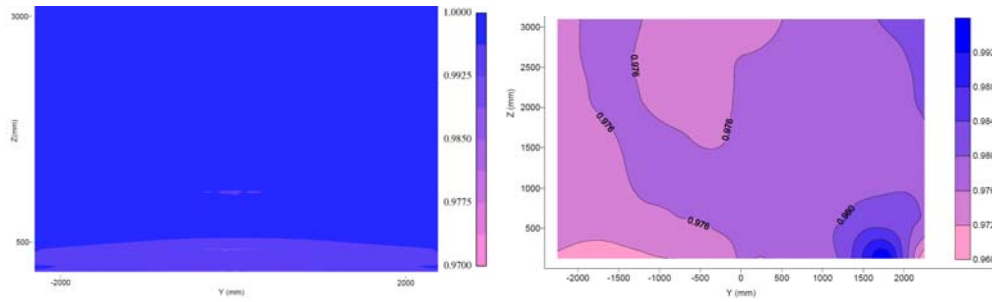


Figure 5.9: Dynamic pressure uniformity at $x=2500$ mm

But then the question arise why the CFD simulation predicts a more uniform flow than what is measured in the experiments? An important reason that cannot be underestimated is the absence of the PVT tunnel's closed air path which have been left out as the simulated geometry has been restricted to the nozzle, test section and diffuser. Even tough turning vanes and turbulence nets are used in the PVT tunnel to make the flow as uniform as possible the flow will inevitable inhabit some non-uniformity when it reaches the nozzle. This non-uniformity is not accounted for in the CFD simulation due to the geometry restrictions and instead a uniform velocity field is enforced at the nozzle inlet, which obviously in not a completely accurate imitation of the true flow conditions.

To find other reason behind the uniformity difference it is interesting to examine how well the CFD modeling of the near wall flow compare to the near wall flow in the experiments. When PVT was calibrated, Aiolos measured the boundary layer at several locations on the floor across the turn table. Four of the locations is illustrated in Figure 5.10 on a top view sketch of the turn table with the center belt, WDU and 2nd suction zone marked. Note that area around position $x=-2710$ mm, which represent stationary floor, is larger on the sketch than in reality. Also, in reality there is a small gap between the static floor and the leading edge of the center belt. In the CFD the static floor and the gap does not exist and the 2nd suction zone directly transcends to the center belt.

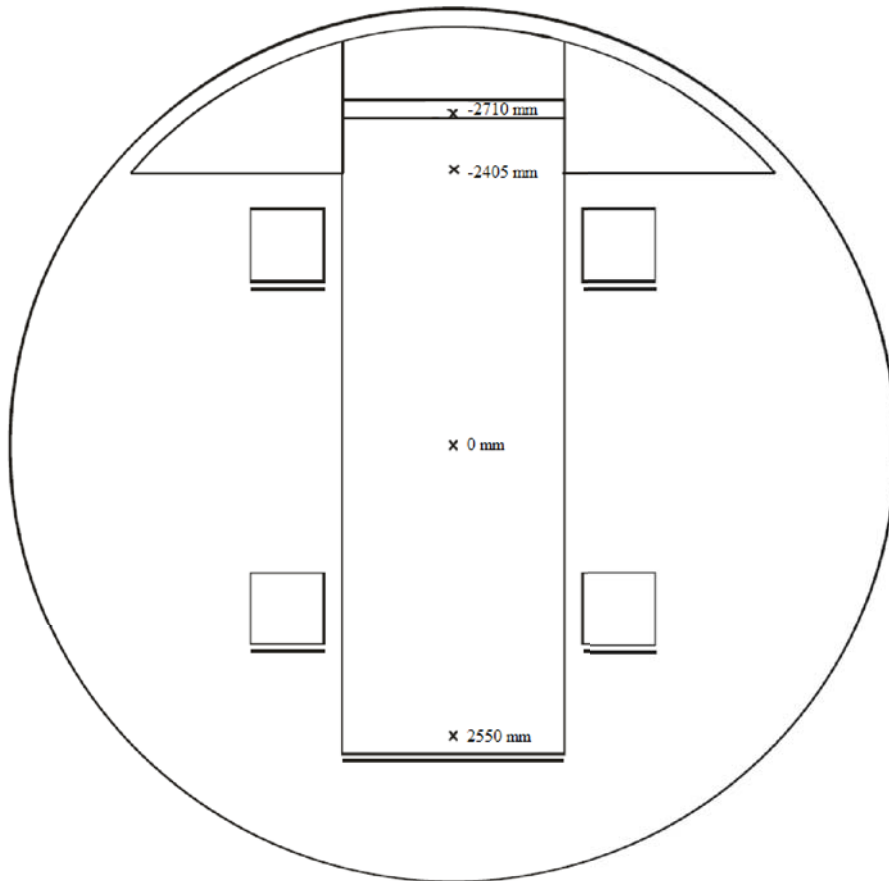


Figure 5.10: Boundary layer measurement locations on the turn table

In Figure 5.11 below the boundary layer on the axial centerline in the four x-positions for Scoop only mode are displayed. The boundary layer grows faster in the CFD than in the experiment but eventually the experiment catches up and 8 meters after the basic suction scoop ($x=-5600\text{mm}$) they are essentially the same. This means that the CFD exaggerates the impact of the wall on the boundary layer development which results in a larger boundary layer thickness in the beginning of the growth of the boundary layer.

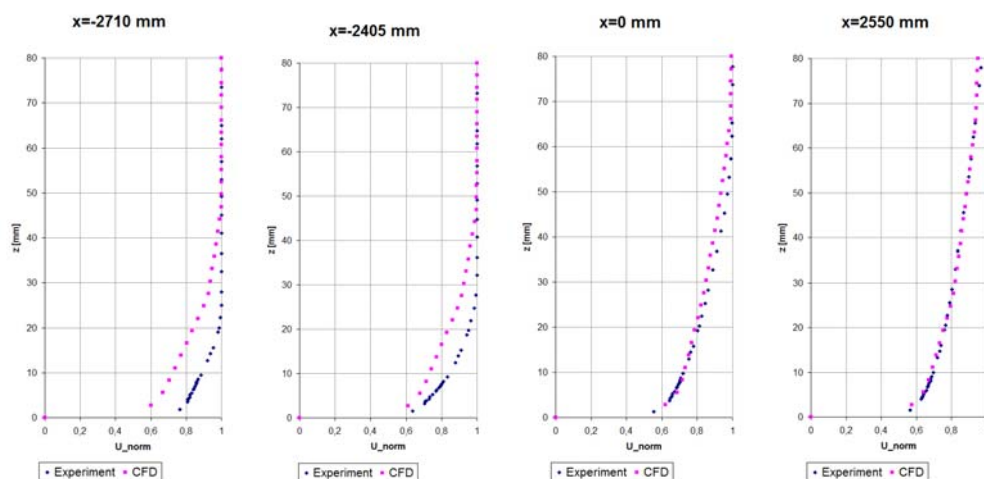


Figure 5.11: Boundary layer profile on the axial centerline across the floor for Scoop only mode

When looking at the boundary layer for the Aerodynamic mode, the impact of the

static floor and the gap between the 2nd suction zone and the center belt is obvious. In the experiment the leading edge of the center belt creates a momentum deficit with a large velocity magnitude across a small height. When it propagates down the center belt the magnitude gets smaller with an increasing height as the flow catches up. As the PVT model in the CFD is simplified with a completely flat floor, this velocity deficit is non-existent due to the absence of any geometry triggering it and the boundary layer never develops along center belt.

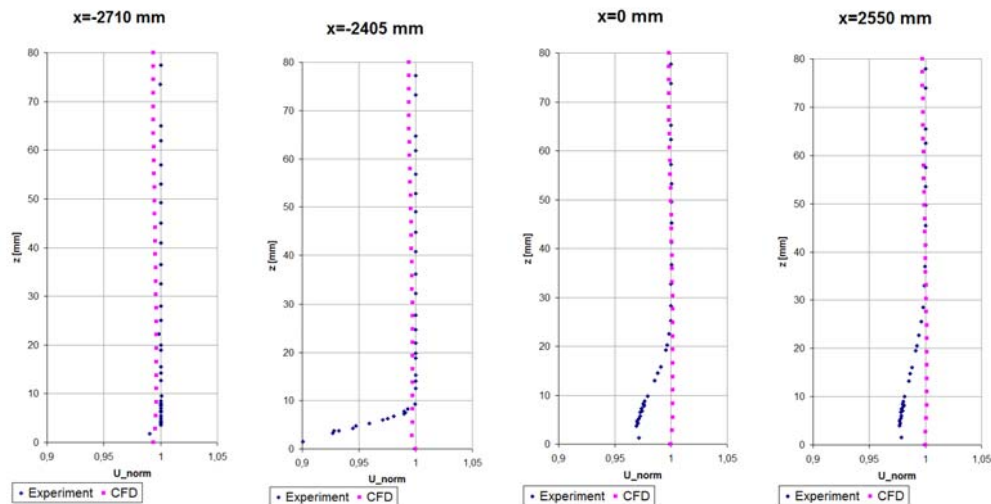


Figure 5.12: Boundary layer profile on the axial centerline across the floor for Aerodynamic mode

The simplification of the floor and the resulting absence of a boundary layer along the center belt is a factor that will help keep the flow uniform. As the simplification of the geometry in the CFD simulation is not restricted to only the floor, but is performed throughout the whole domain, there is a chance that important geometries have been left out which would have had a big influence on the uniformity of the flow and consequently the pressure on the slotted walls.

The discovery of the somewhat irregular pressure drop along the roof center line of the nozzle prompted a brief examination to be made during the experiments performed by Erik Lindmark [9]. Four pressure taps was placed 500 mm to the left of the center line, with the first tap placed 50 mm before P_{C2} , the second tap at the same x-position as P_{C2} and the last two after P_{C2} . The position of the pressure taps can be seen in Figure 5.13. The allocation of the pressure tap before P_{C2} was limited by how far it was possible to reach with the help of the available ladder.

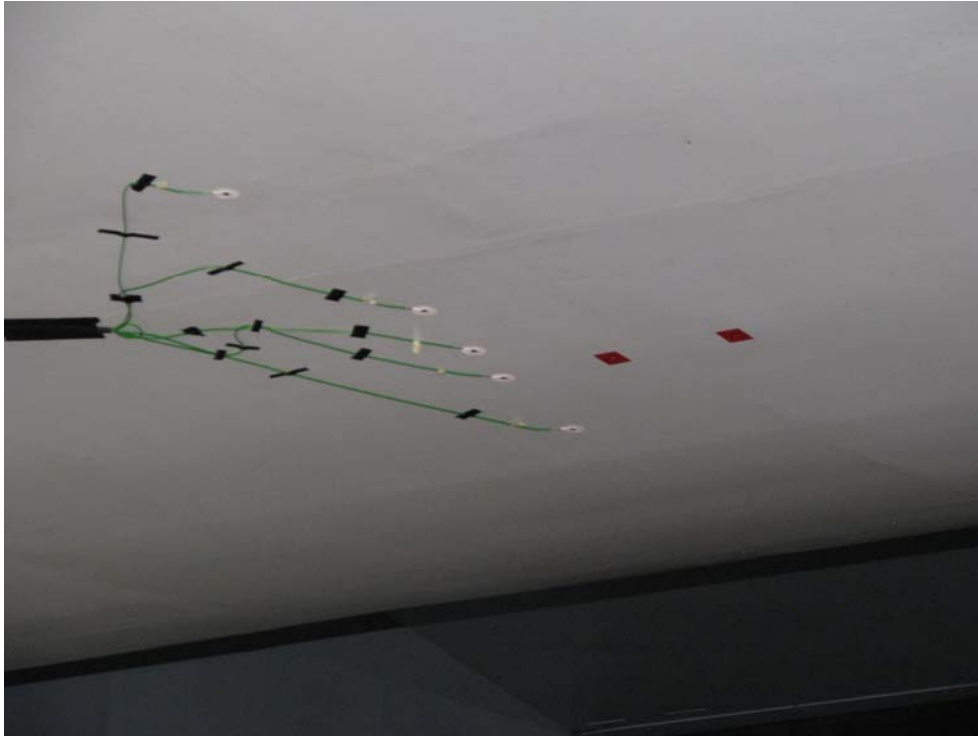


Figure 5.13: Pressure taps on the nozzle roof

The resulting graph of C_p along the pressure tap for an empty tunnel is displayed in Figure 5.14. The graph shows that the pressure reaches its minimum at the pressure tap placed close to C_p , different from the CFD results where the minimum was found 550 mm before P_{C2} . However, in the CFD results the pressure along the whole length of the nozzle roof was plotted and in the experiment only one pressure tap was positioned before P_{C2} , which is not enough to give a true picture of the change in pressure across C_p . The values of C_p is also worryingly high, far from zero when they should be close to zero, especially the second pressure tap, so it is recommended to perform further measurement of the nozzle pressure.

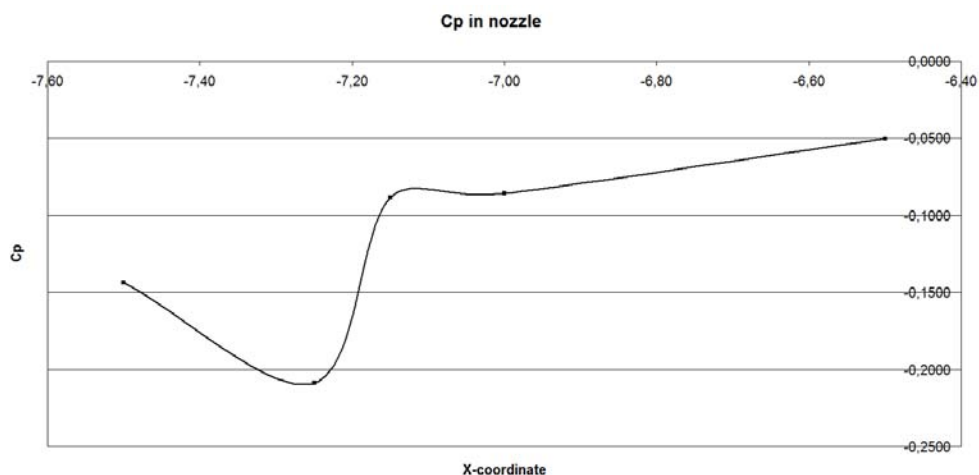


Figure 5.14: C_p on the nozzle roof from experiments

Up till now, only the weaknesses of the CFD simulation have been discussed as reasons behind the difference compared to the experiments and no thought have been put on the errors that comes with the measuring technique during the experiments. These are however

many and sometimes severe but going through them here would demand too much time and space. For sources of error in the experiments performed by Aiolos see the Commissioning report [7].

5.2 Tunnel With Simplified S60

5.2.1 Asymmetrical Behaviour

The asymmetrical geometry's impact on the flow field is more clear when a car is inside the tunnel. Figure 5.15, where C_p is plotted across the 2nd beam element of the slotted walls, shows that the difference between the right and left side is more significant than without a car in the tunnel.

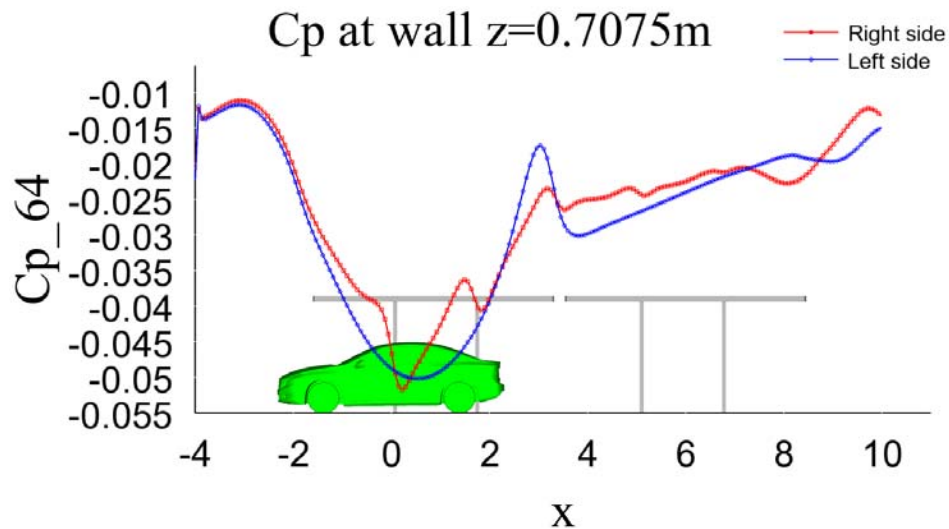


Figure 5.15: C_p at slotted walls with a S60

By looking at the wake of the car the impact of the asymmetry on the flow around the car can be distinguished. In Figure 5.16 the wake 100 mm meters behind the rear of the car is plotted. The wake shows that there is a larger inflow from the left side of the tunnel. Since the flow tends to always move to the area of lowest pressure, more mass flow flows through the slotted walls on the left side of the car where there is less blockage than on the right side. This leads to that more air can flow in behind the car on the left side than on the right side, thus resulting in an asymmetric wake. This is further emphasized by Figure 5.17 which is the wake 1000 mm behind the rear of the car. The wake is even more asymmetric here.

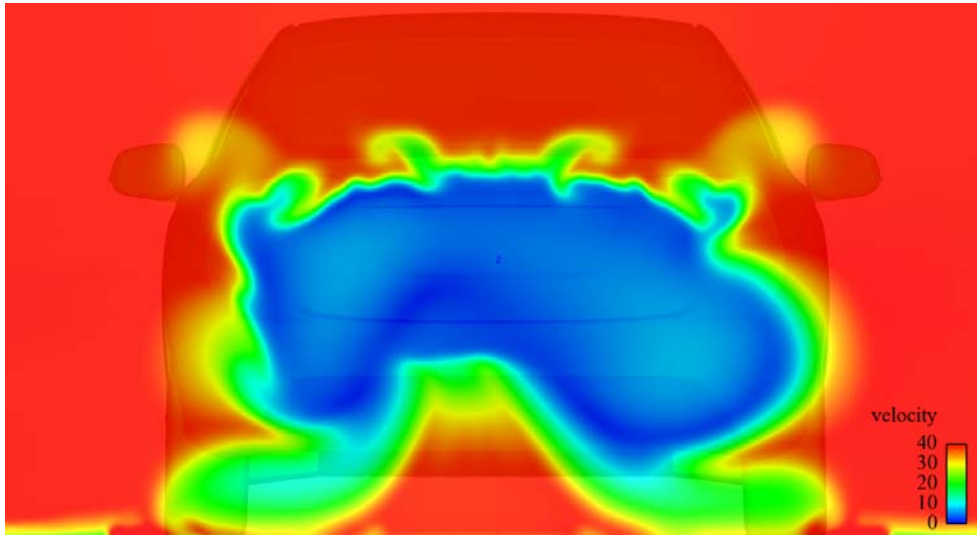


Figure 5.16: S60 wake 100 mm behind the rear of the car in the PVT tunnel

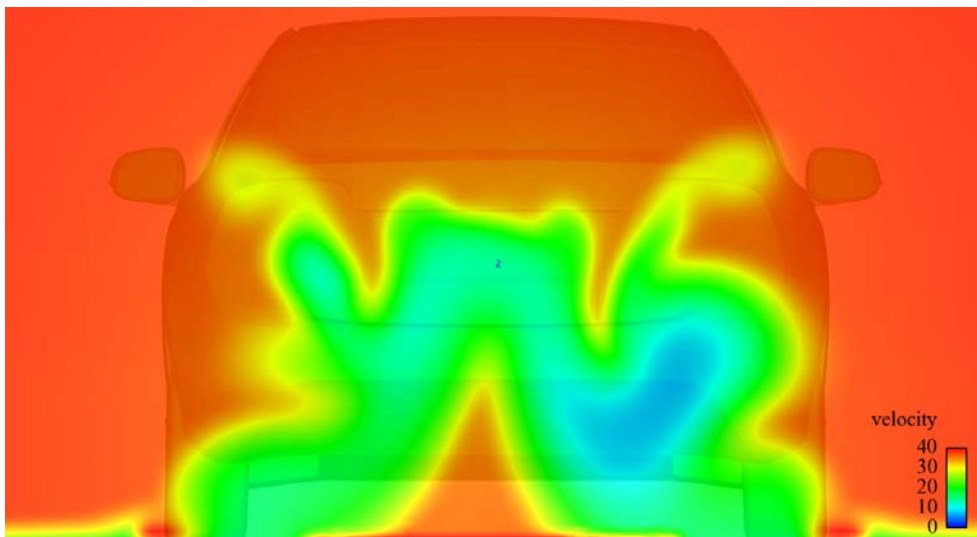


Figure 5.17: S60 wake 1000 mm behind the rear of the car in the PVT tunnel

The amount of mass flow through the slots was measured for each slot and the result for the right and left slots is displayed in Figure 5.18. Since the mass flow have been integrated across the whole length of each slot, the number represent the average mass flow across the slot. A negative value for the left side means that more flow is moving from the inside of the test section to the plenum side and a positive value means that more flow is entering the test section. For the right side the values are of opposite sign and a negative value means that more air is flowing into the test section.

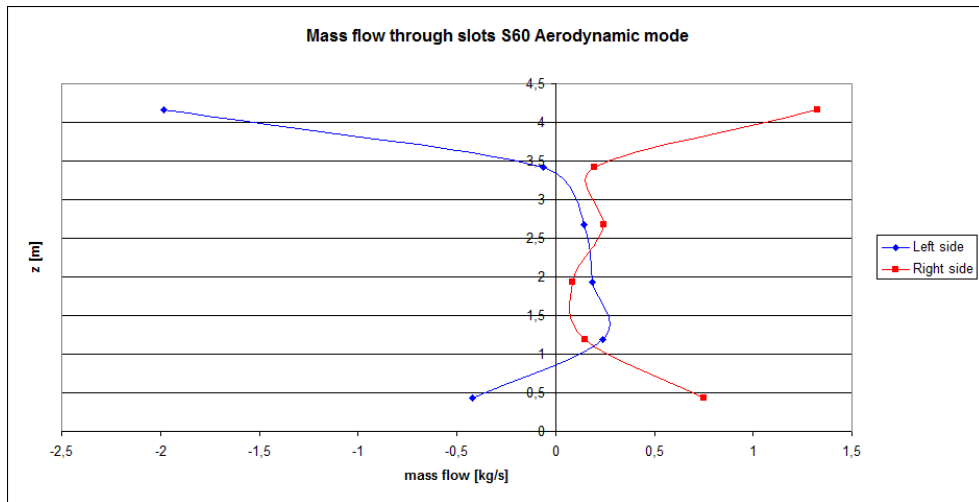


Figure 5.18: Mass flow through the slots on the right and left side

The figure shows that the more flow is leaving the test section than entering it on the right side for all slots. For the left side the opposite occur for slot number 2 to 4 counted from the ground, where number 2 is roughly situated at the waist line of the car and the other two above. This indicates the reason behind the large inflow on the left side, but to get the whole picture it is convenient to look at the elevated surfaces of the mass flow through the slots which is showed by Figure 5.19. The flow is coming back behind the car in a larger scale on the left side compare to the right side which have resulted in the very asymmetric wake.

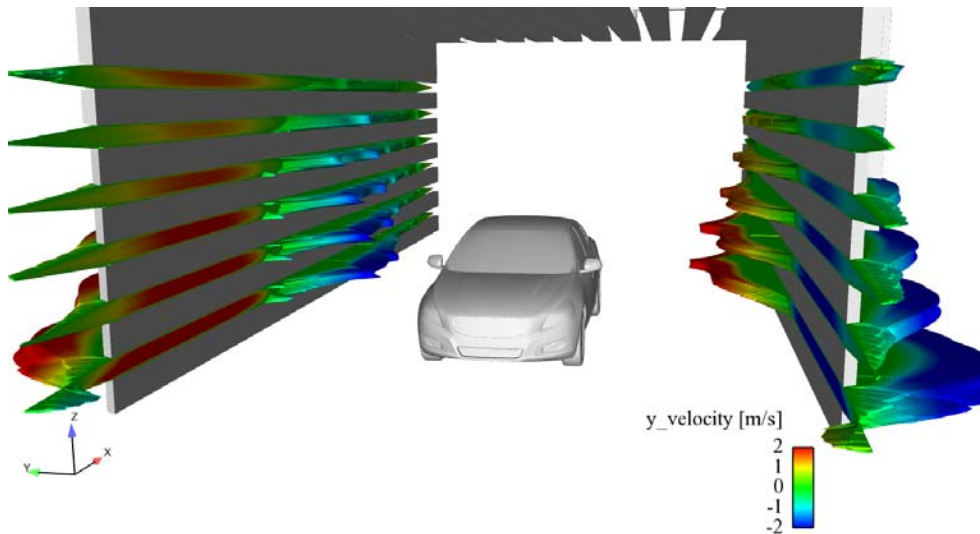


Figure 5.19: Mass flow through the slots represented by elevated surfaces

Shown below in Figure 5.20 and 5.21 is the wake of the car in an ordinary CFD tunnel, which is a large rectangular box with symmetry boundary conditions. The ordinary CFD simulation have also a complete moving ground system instead of a 5-belt system. The wake is here very symmetric which is expected as the car itself is symmetric. The difference between the CFD tunnel and PVT tunnel is quite large, a difference which is not desirable.

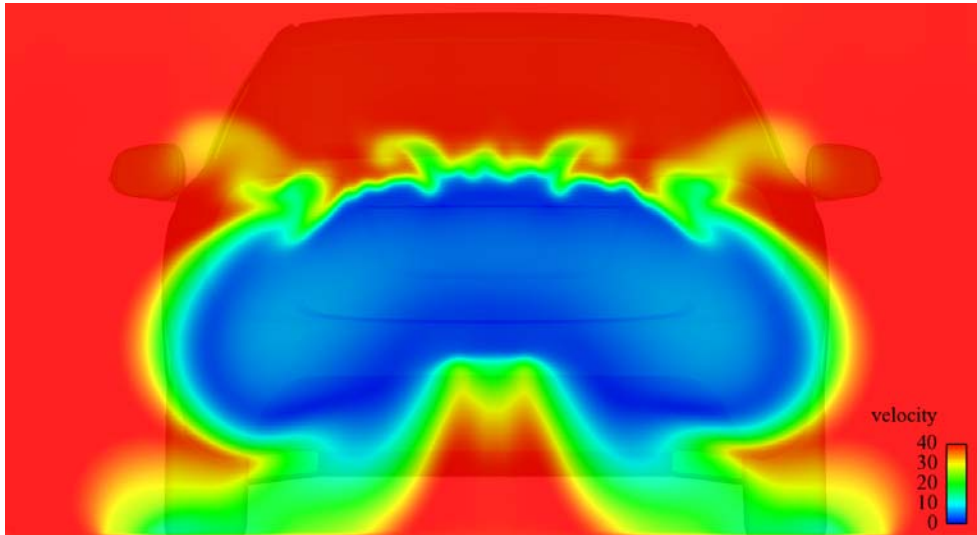


Figure 5.20: S60 wake 100 mm behind the rear of the car in the CFD tunnel

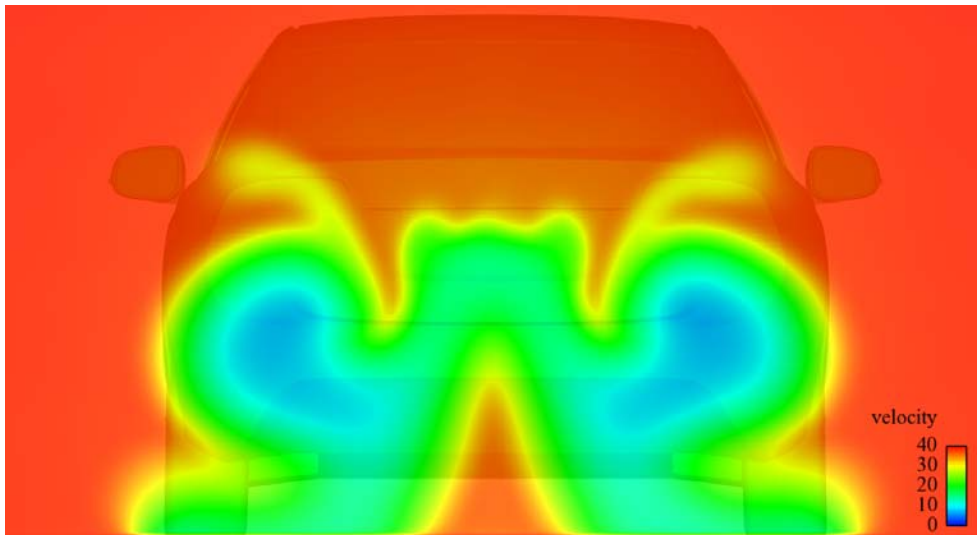


Figure 5.21: S60 wake 1000 mm behind the rear of the car in the CFD tunnel

During experiments in the PVT tunnel there have always been a difference in yawing the car to the left compared to yawing it to the right. With cars with asymmetric floor this could be expected but the difference have been large and the asymmetric floor cannot be the sole reason. Since the CFD simulations have shown that the asymmetric slotted walls in the PVT tunnel have a large impact on the flow, there is good reason to believe that the resulting asymmetry in the flow could be a contributing factor. Therefore simulations was performed with the S60 yawed 20° to the right and yawed 20° to left. Despite the car being symmetric, Figure 5.22 shows a clear difference between the direction of yawing.

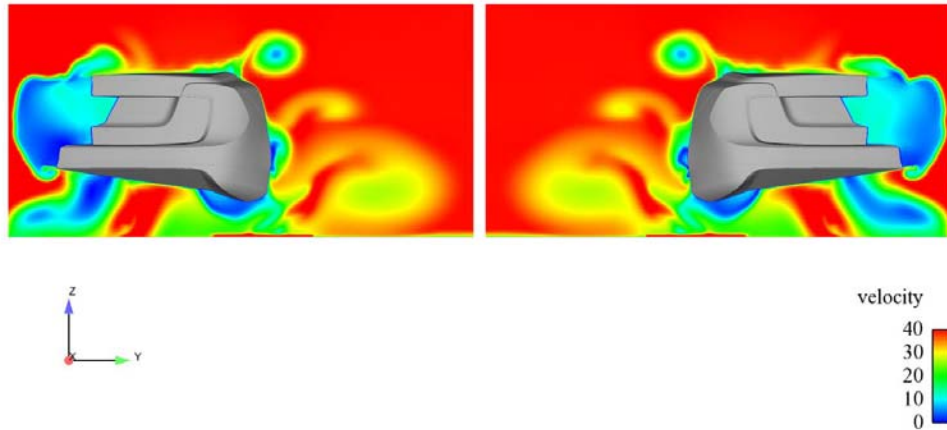


Figure 5.22: Wake comparison of yawing 20° to the right and left

The difference in calculated C_d and C_l values shown in Table 5.1 is the definite proof that the asymmetric slotted walls have a large impact on the result from the PVT tunnel. Especially lift is different which shows that lift is more sensitive to asymmetric flow than drag.

Table 5.1: C_d and C_l for S60 yawed to the right and left

Case	C_d	C_l
+ 20°	0.464	0.157
- 20°	0.470	0.186

5.2.2 PVT Tunnel impact on pressure coefficients

With such a different flow field in the PVT tunnel compared to the CFD tunnel, there should also be different drag and lift coefficients produced. In Table 5.2 the C_d and C_l values are stated for the PVT tunnel and the CFD tunnel. The drag is lower in the PVT tunnel, which is not expected because in reality the experiments always give higher C_d than the standard CFD simulations. The lower drag is partly due to the BLCS mass flow values being set too low in the boundary condition settings but since that probably only result in a few percent too low C_d it cannot be the sole reason and even with the correct mass flow values, the C_d in the PVT tunnel would still be lower than the CFD tunnel.

Table 5.2: The drag and lift coefficient for the S60

Case	C_d	C_l
PVT tunnel	0.241	0.027
CFD tunnel	0.266	-0.044

The reason behind the difference in C_d is found when comparing the base pressure of the car which is shown by Figure 5.23 and Figure 5.24. In the CFD tunnel the base pressure is lower than in the PVT tunnel, which gives a higher pressure drag due to the larger difference in pressure between the front and rear of the car. However, note the lower

pressure on the back of the rear wheels when the car is in the PVT tunnel. The cause behind this will be investigated with the S80 in the tunnel.

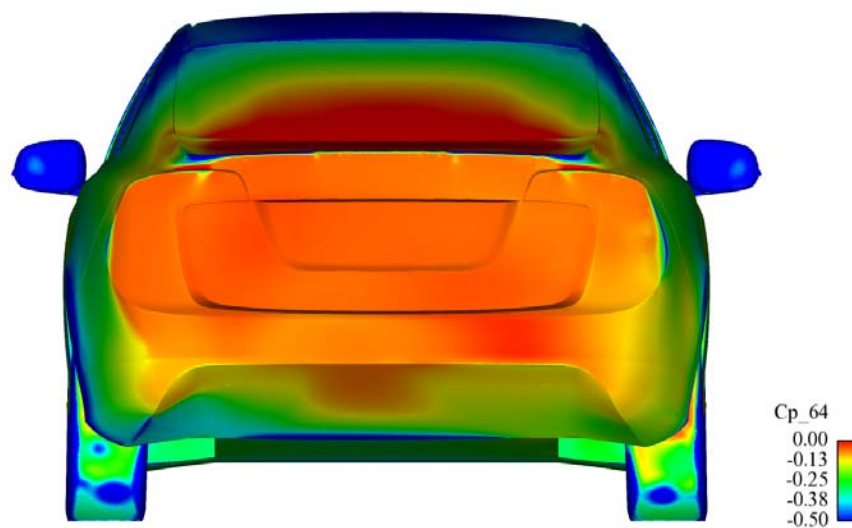


Figure 5.23: C_p at rear of the S60 in the PVT tunnel

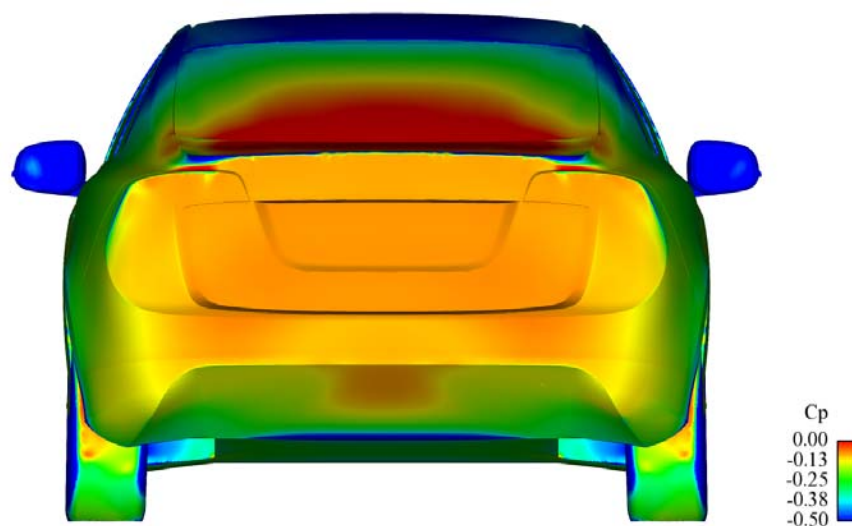


Figure 5.24: C_p at rear of the S60 in the CFD tunnel

The difference in lift is more expected as the simulation of the moving ground is different in the two cases. In the PVT tunnel the open road conditions is simulated by a 5-belt moving ground system and a boundary control system, with different suction zones and tangential blowing. This is very different from the CFD tunnel where the complete ground is set as moving. In order to investigate the impact of the floor in the PVT tunnel a new simulation was performed with the whole floor inside the slotted walls set as moving ground, the same floor boundary condition as in the CFD tunnel. The basic scoop was kept because turning it off would have given strange results due to the large stagnation area created. However, this was only done early in the project with a coarse mesh without any refinement boxes around the S60, which means that the accuracy of the simulations is lower. Table 5.3 shows the drag and lift coefficients for the simulation with Aerodynamic mode and the simulation with complete moving ground.

Table 5.3: C_d and C_l for Aerodynamic mode compared with complete moving ground

Case	C_d	C_l
PVT Aerodynamic mode	0.248	0.030
PVT Complete moving ground	0.257	0.016

The table confirms that the lift coefficient depends largely on the type of moving ground simulation system used. The 5-belt system does not fully simulate moving road conditions and despite using tangential blowing to "fill in" the boundary layer between the wheels, a higher C_l is obtained. That the opposite happen for the drag coefficient is not as easy to explain because a larger area of moving ground should decrease C_d . However, the change from Aerodynamic mode to complete moving ground means also that it is less suction inside the domain and that influences the flow field. The reason behind the lower C_d with Aerodynamic mode will be further investigate with the S80 in the tunnel.

5.3 Tunnel With S80 Closed Front

5.3.1 Asymmetrical Behaviour

Figure 5.25 shows that just as the simple S60, the S80 increases the difference of C_p on the right side compared to the left side of the slotted walls. Compared to the S60 the largest difference is found at the end of the walls, which implies that the wake structure is different. That is something which is expected as the S80 has a different body and a detailed, unsymmetrical floor.

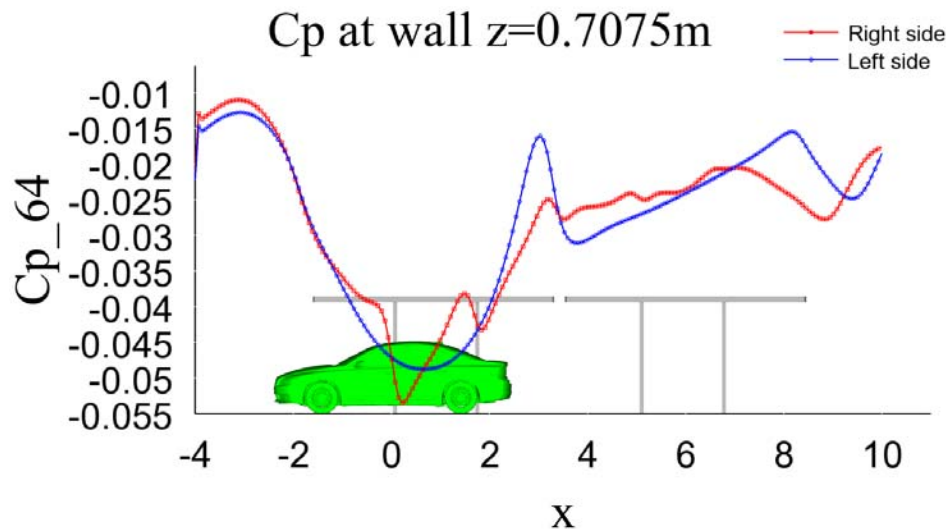


Figure 5.25: C_p at slotted walls with a S80

What was not expected though, was that the wake of the S80 would be more symmetric in the PVT tunnel compared to the CFD tunnel. The results from the PVT tunnel is shown by Figure 5.26 and Figure 5.27 and the results from the CFD tunnel is shown in Figure 5.28 and Figure 5.29. The difference is most notable at the top and bottom of the wake, which represents the flow coming from over and under the car. It seems like the asymmetry of the slotted walls even out the effect of the asymmetric floor and vice versa. There is no large inflow from the left side like in the case with the S60. Apparently some of the information regarding the asymmetry of the flow around a car is lost in the PVT tunnel.

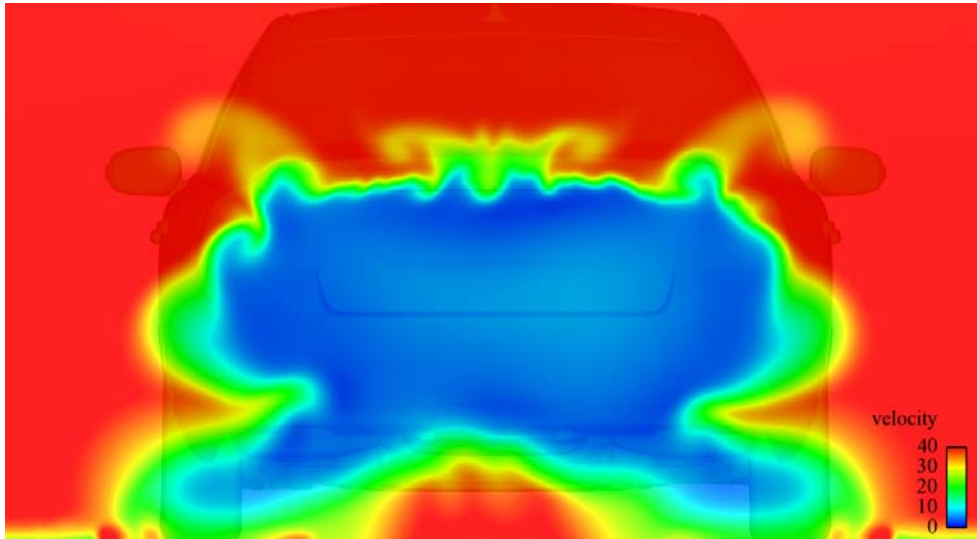


Figure 5.26: S80 wake 100 mm behind the rear in the PVT tunnel

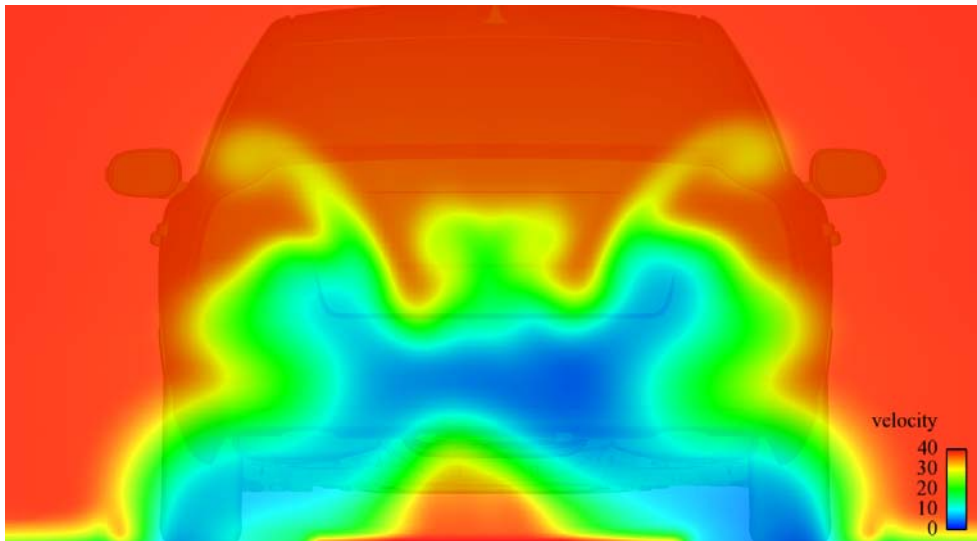


Figure 5.27: S80 wake 1000 mm behind the rear in the PVT tunnel

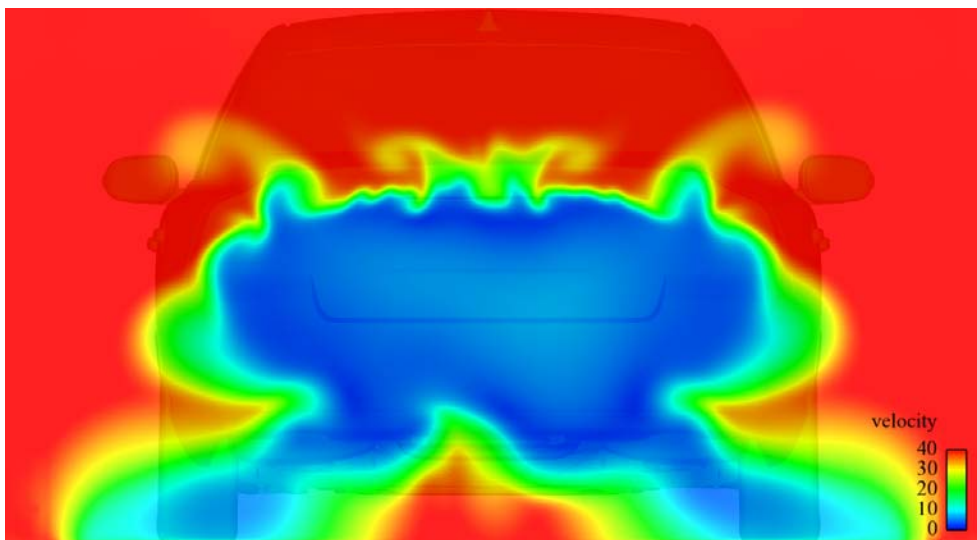


Figure 5.28: S80 wake 100 mm behind the rear in the CFD tunnel

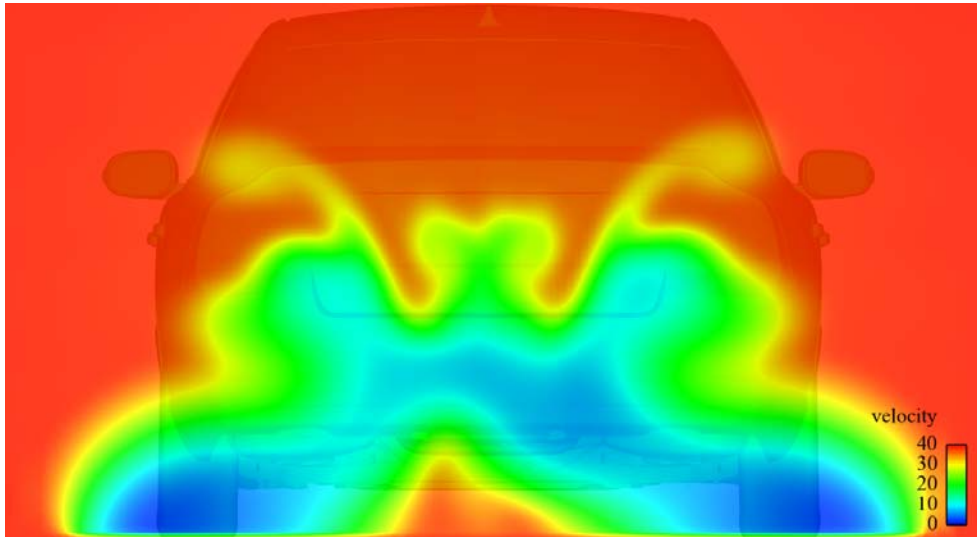


Figure 5.29: S80 wake 1000 mm behind the rear in the CFD tunnel

This is further emphasized by Figures 5.30 and 5.31 where C_p on the top of the car is plotted. At the windscreen junction the pressure on the car is very symmetric when the car is in the PVT tunnel, but less so in the CFD tunnel. The impact of the tunnel walls is in this case counter productive and the results from the PVT tunnel does not give a completely true picture of the flow around the car.

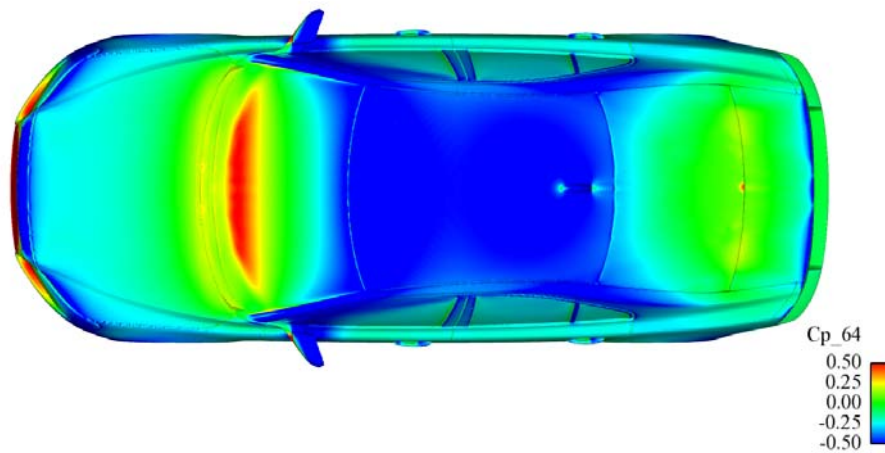


Figure 5.30: C_p on the top of the S80 in the PVT tunnel

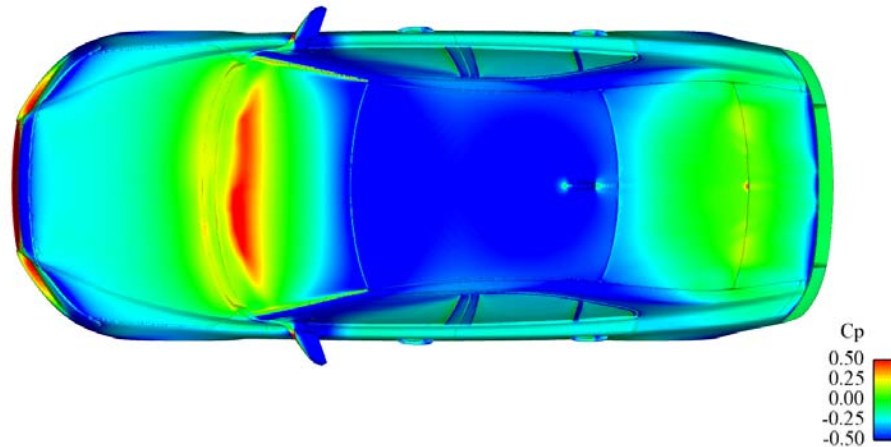


Figure 5.31: C_p on the top of the S80 in the CFD tunnel

In order to investigate the tangential blowing's effect on the drag, covered in the next chapter, a new simulation was performed with the tangential blowing turned off. As supported by Figure 5.32, where the wake 100 mm behind the rear of the car is shown, without the tangential blowing the flow coming from the top of the car is a lot more asymmetric. The vortexes which is created by the radio antenna on the roof is different on the left side compared to the right.

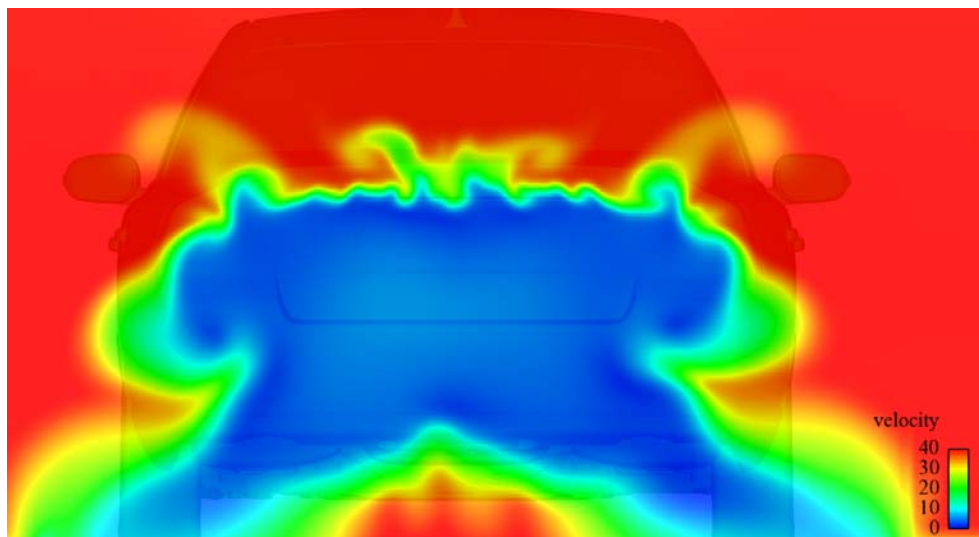


Figure 5.32: S80 wake 100 mm behind the rear in the PVT tunnel with the tangential blowing deactivated

5.3.2 PVT Tunnel impact on pressure coefficients

From earlier experience at Volvo Cars the CFD calculations always produced lower C_d values than the experiments in the PVT tunnel. It should therefore be expected that the simulation of the PVT tunnel would give a higher C_d than the simulation of a CFD tunnel. However, the result follow the same pattern as the S60 and the S80 in the PVT simulation have a lower C_d than in the CFD simulation. The C_d and C_l values are shown in Table 5.4.

Table 5.4: The drag and lift coefficient for the S80, PVT tunnel versus CFD tunnel

Case	C_d	C_l
PVT tunnel	0.279	0.135
CFD tunnel	0.284	0.127

One of the reason behind the higher C_d in the CFD tunnel is because of the lower base pressure on the car. The base pressure of the PVT tunnel and the CFD tunnel is shown in Figure 5.33 and Figure 5.34 respectively. Red colour indicates C_p values close to zero and the area of red colour is larger on the S80 in the PVT tunnel which means that the base pressure is higher, giving a lower C_d . But in the PVT tunnel the pressure is also lower on the backside of the rear wheels which should contribute to an increase in drag. There is obviously something in the PVT tunnel which lowers the pressure on the back of the rear wheels but not enough to counteract the higher base pressure.

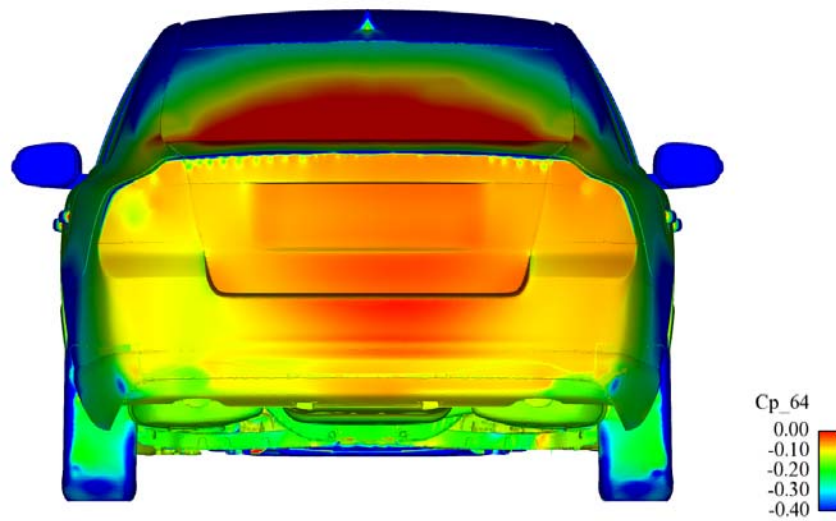


Figure 5.33: Base pressure of the S80 in the PVT tunnel

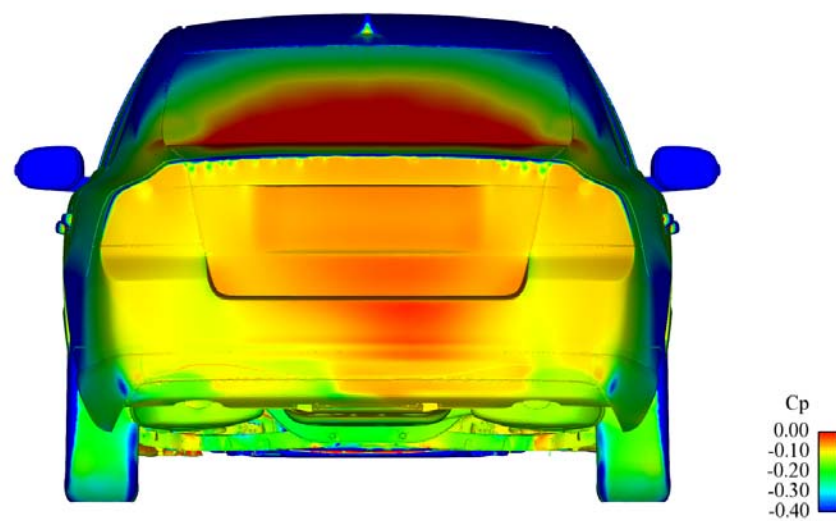


Figure 5.34: Base pressure of the S80 in the CFD tunnel

One contributing factor to drag is found when the losses are examined by looking at areas where total pressure equals zero. The corresponding isosurfaces of total pressure equals zero is shown in Figure 5.35 and Figure 5.36 for the PVT tunnel and CFD tunnel respectively. The pictures shows that the losses after the wheels are bigger in the CFD tunnel than in the PVT tunnel which partly explains the higher C_d .

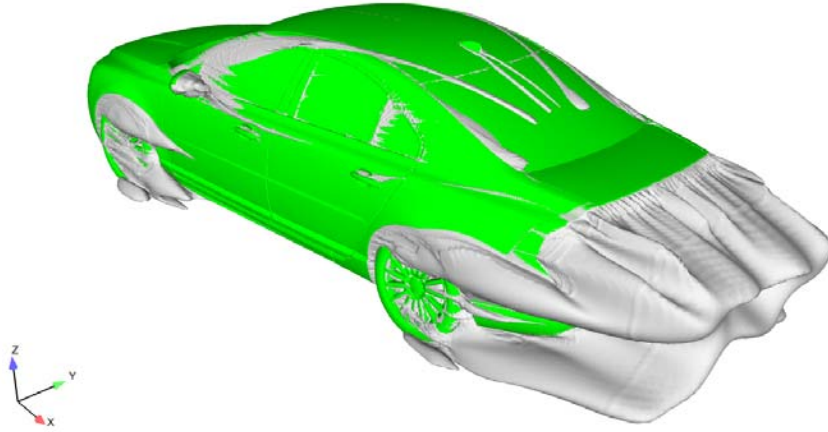


Figure 5.35: Isosurface of total pressure equals zero for PVT

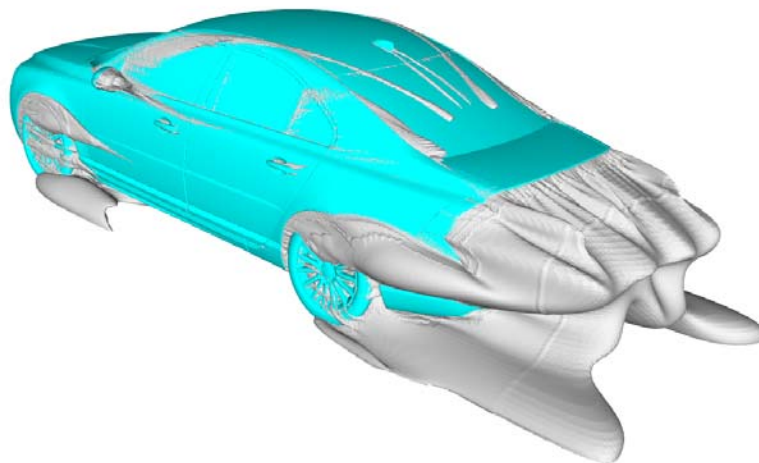


Figure 5.36: Isosurface of total pressure equals zero for CFD

It seem like the tangential blowing in the PVT tunnel removes part of the wake structure behind the wheels due to its insertion of high energy flow. It is therefore of interest to examine the impact of the tangential blowing more closer. Figure 5.37 illustrates the effect of the tangential blowing behind the left rear wheel of the S80 by showing the velocity magnitude and the velocity vectors. The long, rectangular surface behind the wheel is the inlet area of the tangential blowing and the inserted high velocity jet pulls down the air behind the rear wheel, thus lowers the pressure.

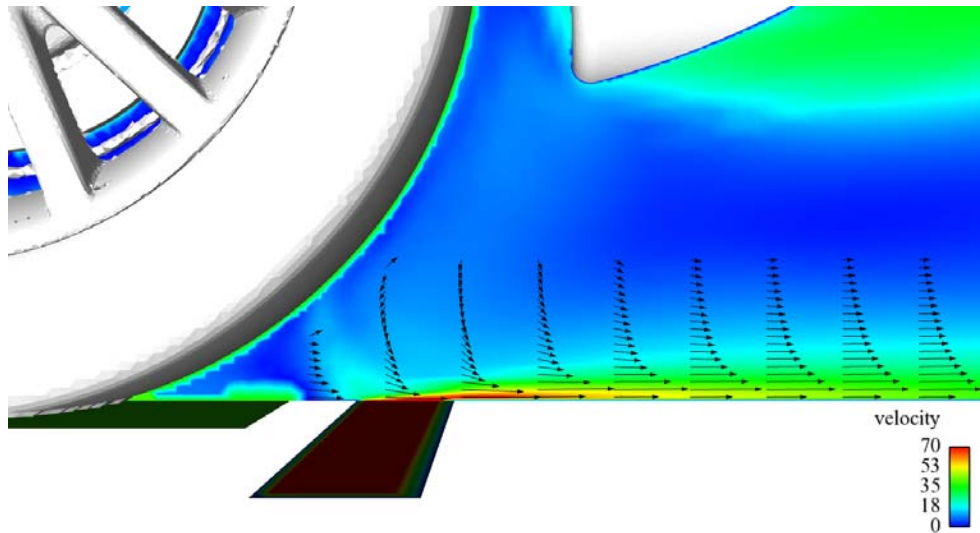


Figure 5.37: Velocity contour and vectors behind rear wheel

The tangential blowing is used to "fill in" the boundary layer that have started to build up behind the WDU, with the aim of having a integrated boundary layer displacement thickness of zero at some point downstream of the inlet. However, the velocity vectors and velocity contour indicates that the tangential blowing acts across a height larger than anticipated, a feat caused by the very high inlet velocity of the jet. In order to investigate the impact of the tangential blowing on the drag, a new simulation was performed with the tangential blowing turned of. The resulting velocity field and vectors behind the rear can be seen in Figure 5.38. There is no insertion of high energy flow and the wake behind the rear wheel extends all the way down to the floor. Note also that the direction of the flow above the tangential blowing area is now concentrated to the x-direction, different from when the tangential blowing is activated and the flow is drawn down by the inserted high speed flow.

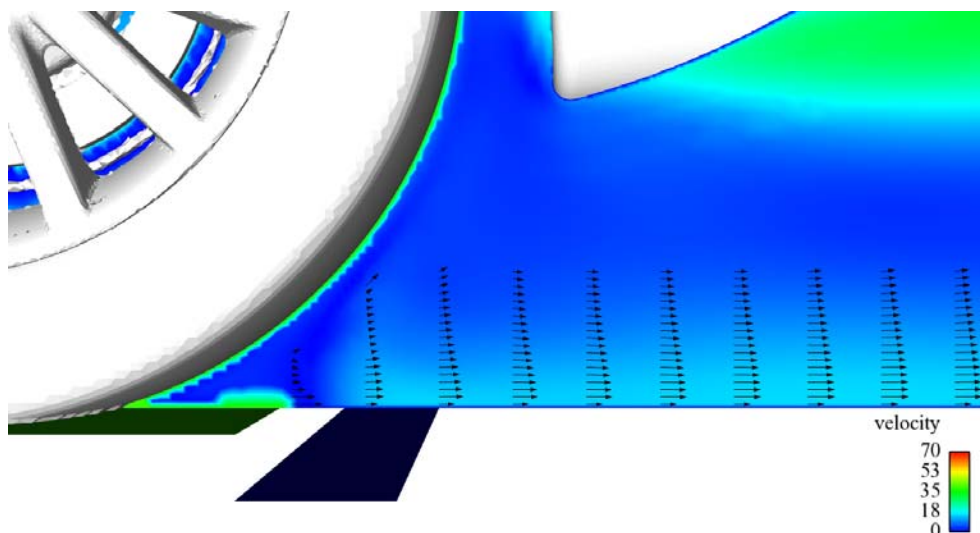


Figure 5.38: Velocity contour and vectors behind rear wheel with the tangential blowing deactivated

To fully understand how the tangential blowing changes the flow field, it is convenient to look at the stream lines behind the rear wheels. In Figure 5.39 the trailing vortexes behind the car is accelerated by the insertion of high energy flow from the tangential blowing. With the tangential blowing turned off the vortexes is less strong, as shown by Figure 5.40, and a wake forms due to the very low velocity of the swirling flow just after the rear wheels.

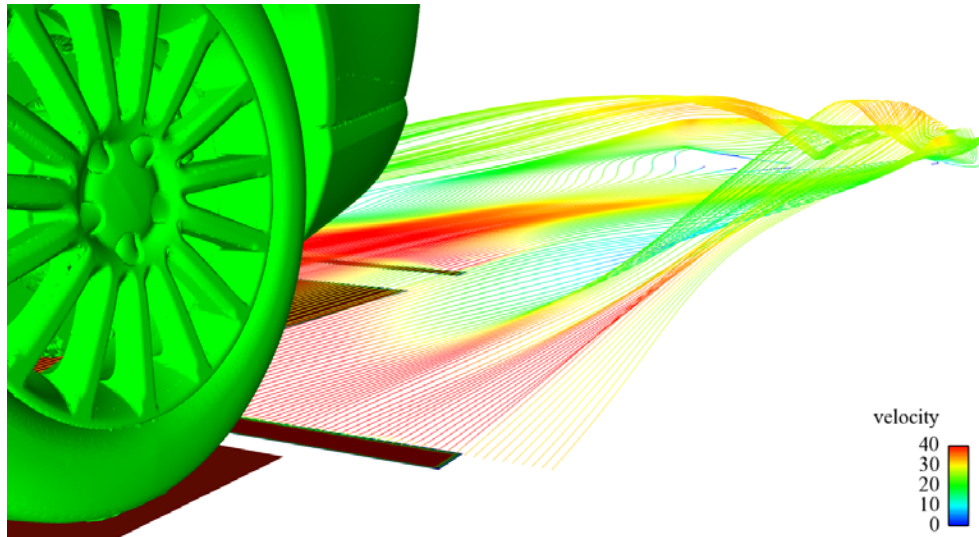


Figure 5.39: Streamlines behind the car showing the impact of the tangential blowing

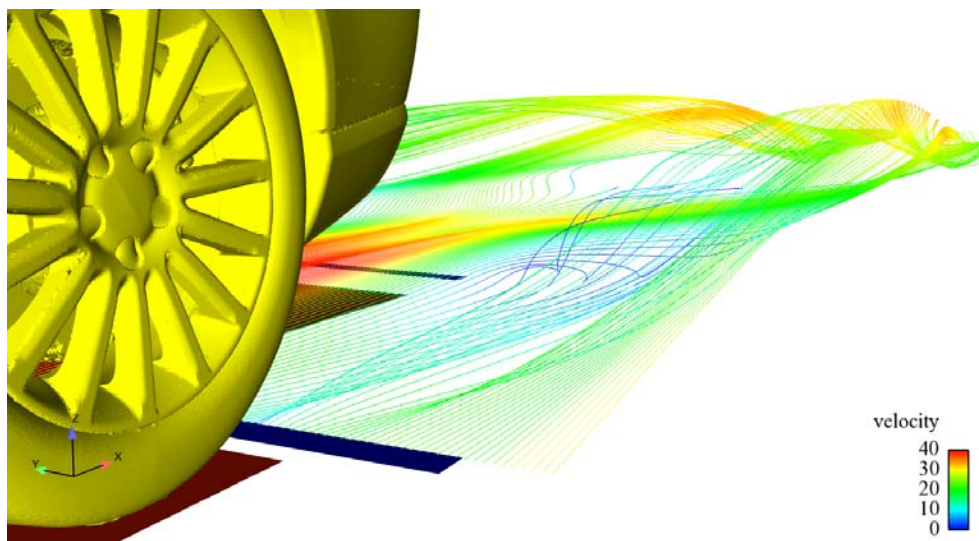


Figure 5.40: Streamlines behind the car with the tangential blowing turned off

With the tangential blowing turned off, the wake structure is now more like the one from the CFD tunnel, as seen by Figure 5.41. More losses occur behind the wheels, especially behind the rear wheels. Based on this increase in losses one would expect a higher drag coefficient, but actually the opposite happen as the deactivation of the tangential blowing further lowers the C_d as stated by Table 5.5.

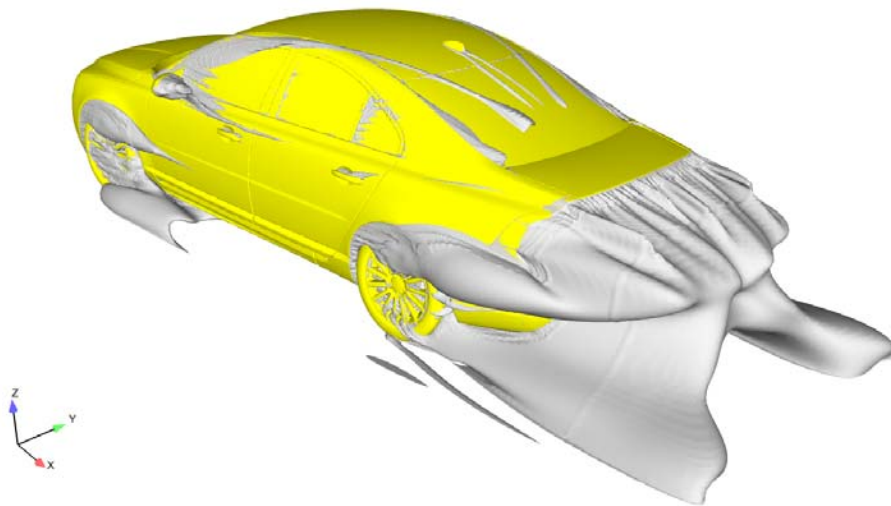


Figure 5.41: Isosurface of total pressure equals zero for PVT with the tangential blowing turned of

Table 5.5: The impact of tangential blowing on drag and lift coefficients for the S80

Case	C_d	C_l
PVT tunnel	0.279	0.135
PVT tunnel without tangential blowing	0.272	0.168

This is because even tough the wake structure becomes larger with the tangential blowing turned of, it is made obsolete by the decrease in stagnation pressure on the front of the rear wheel, as seen by comparing Figure 5.42 and 5.43, which shows the pressure on the forward facing part of the car with tangential blowing turned on and off respectively. The larger stagnation pressure on the rear wheels together with the lower pressure behind the rear wheels when the tangential blowing is activated, contributes to an increase in drag. This behavior is very well matched with observations from experiments in the PVT tunnel.

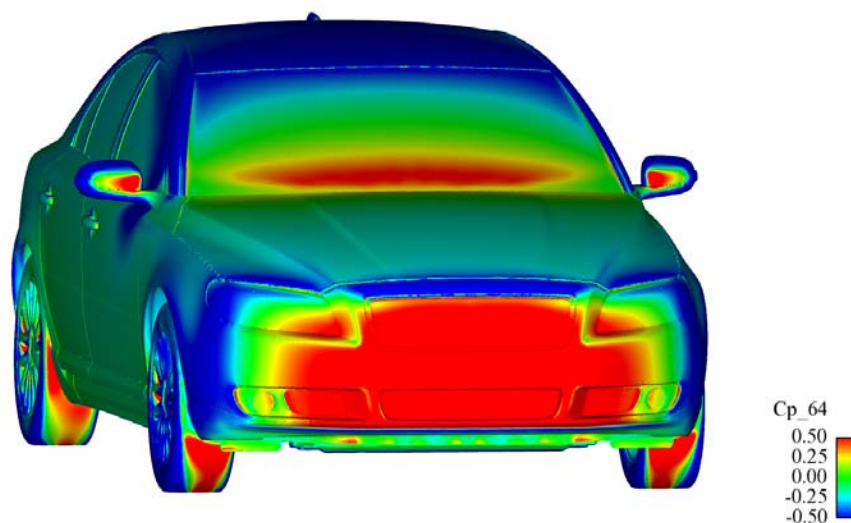


Figure 5.42: C_p of the forward facing areas of the S80 with tangential blowing turned on

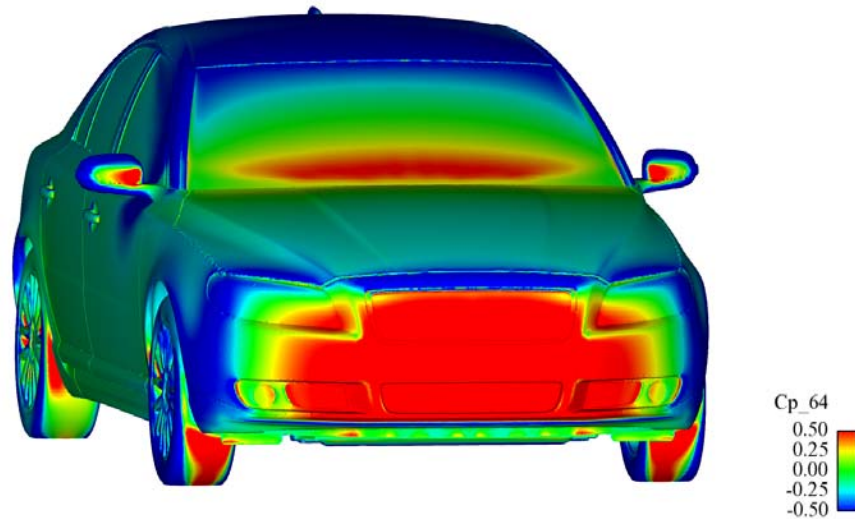


Figure 5.43: C_p of the forward facing areas of the S80 with the tangential blowing turned off

5.3.3 Comparison With Experiments

The closest experiment possible to compare with the S80 closed front CFD simulation was the 2007 S80 with the front grill and spoiler opening taped, performed by former thesis worker James C. Lyon [8]. Even though a taped grill and spoiler means that no air is allowed into the engine bay and cooling package through the front, air can still enter through the openings of the floor. This means that some differences between the CFD results and the experiments should be expected. Table 5.6 displays the drag and lift coefficients from the experiment and the CFD calculation. The difference is quite large, a bit larger than expected, and has its source in the differences already experienced in the empty tunnel.

Table 5.6: The drag and lift coefficient for the S80 closed front, CFD versus experiment

Case	C_d	C_l
PVT simulation	0.279	0.135
Experiment	0.308	0.187

Another hint of the reasons behind the differences between the CFD and experiment is given when comparing the centerline pressure across the S80. The centerline pressure is plotted in Figure 5.44 and there are several disparities found. The pressure is consequently predicted higher in the CFD compared to the experiment, regardless of sign. However, care should be taken when analyzing this figure, since the two cases are different as explained previously in this section. Also, as explained in the subsection Post Processing of the section Method, the way C_p have been calculated differs and the positions of the pressure points have been approximated.

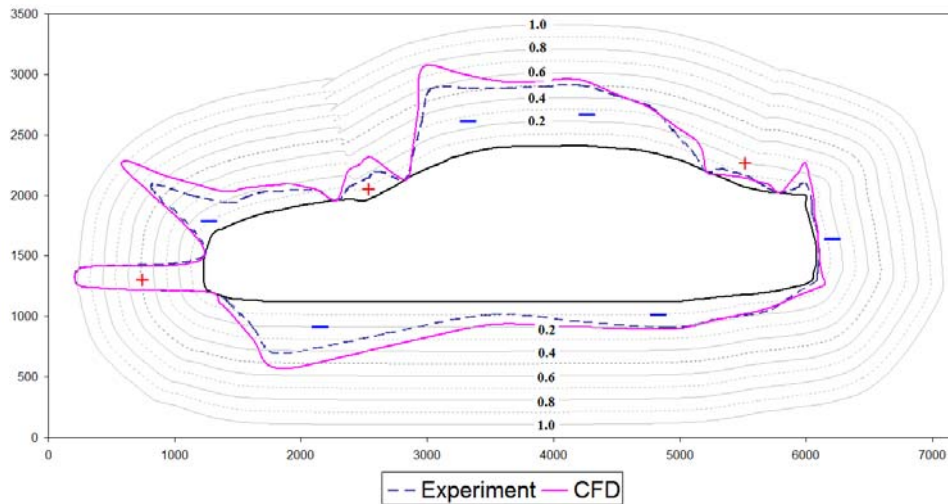


Figure 5.44: C_p across the centerline of the S80 for CFD vs experiment

5.4 Tunnel With S80 Open Cooling

The PVT simulations with the S80 open cooling had during completion of this report not been adjusted to the same pressure drop over the nozzle as the empty tunnel. The pressure drop is slightly lower, hence the car is experiences a lower velocity than 140 kph.

5.4.1 PVT Tunnel impact on pressure coefficients

The simulation of the S80 open cooling in the PVT tunnel produces higher drag values than the simulation in the CFD tunnel, but only with a slight margin as stated by Table 5.7. The result is still well below the expected values (see Table 5.8) and the reasons are the same as for the S80 closed front. It seems though that the increase in blockage caused by a larger car or a more detailed car, increases the drag more in the simulation of the PVT tunnel than in the CFD tunnel. This is because the blockage due to the tunnel walls in the PVT tunnel is enhanced by a larger car while the effect in the CFD tunnel is small since there exist no walls.

Table 5.7: The drag and lift coefficient for the S80 open cooling, PVT tunnel vs CFD tunnel

Case	C_d	C_{lf}	C_{lf}
PVT tunnel	0.301	0.127	0.032
CFD tunnel	0.295	0.040	0.115

One interesting observation is that the distribution of lift is the opposite in the PVT tunnel compared to the CFD tunnel. In the PVT tunnel the lift is concentrated to the front of the car where in the CFD tunnel the lift is concentrated to the rear of the car. Reason behind this is not investigated in this master thesis due to time constrains.

5.4.2 Comparison With Experiments

The S80 with open cooling is a more similar simulation to the real life experiments than the S80 closed front, even tough the approximations in the modelling of the radiators and fans introduces some differences. The drag and lift for the PVT simulation is compared in Table 5.8 with experiment performed by thesis worker Erik Lindmark in 2011 [9]. The

difference between the calculated C_d compared to the measured C_d is smaller than for the S80 closed front model, 25 drag counts compared to 29 drag counts, but the CFD still predicts a lower drag value. The lower lift in the PVT simulation is mainly because of the simplified floor.

Table 5.8: The drag and lift coefficient for the S80 open cooling, CFD versus experiment

Case	C_d	C_l
PVT simulation	0.301	0.160
Experiment	0.326	0.231

In Figure 5.45 C_p across the 2nd slot of both walls for the CFD of the S80 open cooling and the experiment is plotted. The curves follows the same pattern but is of less magnitude in the CFD compared to the experiment. This is a consequence of the large magnitude difference when the tunnel is empty. The way C_p changes when the S80 is put into the tunnel compared to an empty tunnel is similar in the CFD and experiment. There are strong reasons to believe that the curve with a car in the tunnel would have been much more similar, if the experiment with an empty tunnel had shown a varying pressure of the same small magnitude as in the CFD (or the other way around).

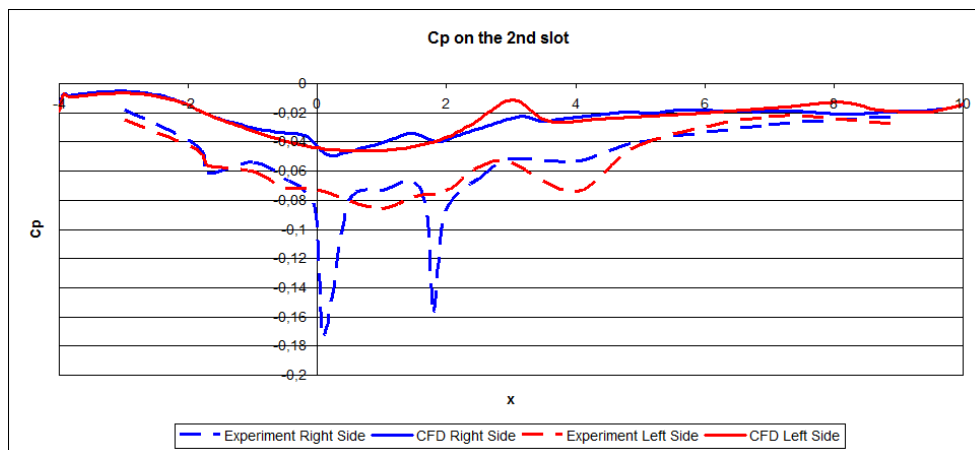


Figure 5.45: C_p for CFD vs experiment

The experimental measurements in Figure 5.45 is the final proof of the asymmetry of the flow in the PVT tunnel.

6 Conclusions

The results have clearly demonstrated that the PVT tunnel has a very unsymmetrical flow field which have a effect on the results, especially when yawing a car in the tunnel, but also during tests when the car is positioned in a straight line. The main reason behind this is the asymmetric support structure of the slotted walls which unfortunately is heavily incorporated in the core structure of the slotted walls.

The asymmetric behaviour has different effect on the flow field depending on what type of car is in the tunnel and how unsymmetrical the floor of the car is. A completely symmetric car, as the S60 model used in this master thesis, is greatly effected since the choice of side which the approaching air will pass the car on is only dependent on the asymmetry of the support structure. This results in a large inflow on the left side of the car which creates a very unsymmetrical wake.

When a S80 with a detailed floor is in the tunnel, the flow is not only affected by the walls but also by the asymmetric floor of the car and the effect from these two suppresses each other, giving a more symmetric flow than what it is believed to be in reality.

The drag coefficients have consistently been lower in the PVT tunnel compared to the the experiments but also lower than the CFD tunnel for all simulations except the S80 open cooling. The reason behind this is probably because of the absence of the complete closed air path of the wind tunnel and several details of the geometry in the test section which if incorporated would have created a less uniform flow, closer to the uniformity measured in the experiments. The more uniform flow caused by the simplification of the simulated geometry gives a less varying pressure across the whole tunnel in the CFD compared to the experiment, especially for the empty tunnel. This is demonstrated by the C_p plots of the slotted walls which shows large differences when the tunnel is empty but less differences when a car is in the tunnel, a feat which suggests that it is the geometry and not the approximations in the CFD which is the source.

Reasons behind the general higher drag values of the experiments in the PVT tunnel was hard to distinguished since the CFD of the PVT tunnel did not replicate this characteristic, but instead produced the opposite. However, a interesting observation made was that the C_d was lowered considerably when the tangential blowing was deactivated. The tangential blowing could be a contributing factor to the high drag values in the experiments, but this needs to be further investigated.

7 Recommendations and Future Work

Since the asymmetry of the walls have showed to be of significant matter, Volvo Cars should consider modifying the support structure of the slotted walls in order to decrease the asymmetry of the flow. At least all object and items that are currently placed behind the slotted walls and which have no important reason for being there, should be removed as they could be influencing the flow.

As the simulations have shown that the flow is a lot more uniform compared to the experiment, the next step in the simulations should be trying to replicate the inlet flow conditions currently experienced in the PVT tunnel. This can be done by using measurements from the tunnel and choosing user defined inlet condition in Fluent. It is also important to consider implementing a larger part of the wind tunnel, presumably the bends and turning vanes of the tunnel, which probably have a significant effect on the flow field. The simulation should be concentrated on an empty tunnel since the empty tunnel is the source of the differences between the PVT simulations and the experiments.

A more thorough study of the PVT tunnel calibration coefficients should be conducted since they are the basis of important variables such as the pressure coefficient. This is done by performing several simulations of an empty tunnel with different velocities and then performing the regular calibration process for each velocity. New calibration coefficients can then be calculated and their velocity dependency can be distinguished.

The option of using a complete moving ground, meaning a belt which width extends all the way to the slotted walls, have been briefly studied during this master thesis. More work should be carried out regarding this, because using a complete moving ground instead of the 5-belt moving ground system and boundary layer control system would greatly simplify the simulation and remove any uncertainties regarding modeling of the floor.

During this master thesis simulations have been performed with several mesh sizes ranging from 30 million cells to above 100 million cells. The calculation expenses have been found to be rather cheap, at the longest 15 hours on 180 CPUs for the S80 open cooling which had a cell size of 114 million cells. But the memory demand with increasing mesh size have showed to be a real problem, with Fluent already needing 64 gigabyte worth of RAM to be able to load the 114 million mesh. It is therefore recommended to limit the amount of cells depending of the available memory on the computer used.

The newer versions of Harpoon (4.2a, 4.3a) have showed to be a lot quicker than the older version 4.1a, especially regarding creation of prism layers where they have been around five times quicker. But care should be taken when using version 4.3a as two weeks was lost during this master thesis because of mesh related convergence problems that was solved by simply using version 4.1a instead.

When using Enight it is recommended to use scripts and journal files as much as possible since Enight can occasionally crash, a feat more frequent when more than one case have been loaded. It is therefore easier if plots and figures can be produced without the need of opening Enight.

References

- [1] J. Sterneus, T. Walker & T. Bender *Upgrade of the Volvo Cars Aerodynamic Wind Tunnel* Technical Paper 2007-01-1043, 2006
- [2] Peter Mlinaric *Investigation of the Influence of Tyre Deformation and Tyre Contact Patch on CFD Predictions of Aerodynamic Forces on a Passenger Car* Master Thesis performed at Volvo Cars, Chalmers University of Technology 2008
- [3] *Ansys Fluent User's Guide* Release 12.0, 2009-01-29
- [4] H. K. Versteeg & W. Malalasekera *An Introduction to Computational Fluid Dynamics, The Finite Volume Method* 2nd edition, Pearson Education Limited 2007
- [5] Volvo Cars *AEDCAE01: Aerodynamic performance assesement of a car exterior with closed front* 2009-09-09
- [6] Volvo Cars *AEDCAE02: Aerodynamic performance assesement of a car exterior with open front* 2009-09-09
- [7] Trevor J. Bender *Commissioning Report: PVT Ground Simulation Upgrade* Internal Technical Report at Volvo Car Corporation 2006
- [8] James C. Lyon *Automobile Aerodynamics on the Road and in the Wind Tunnel - A Correlation Study* Master thesis performed at Volvo Cars, KTH, 2008
- [9] Erik Lindmark *Analysis of Pressure Measurements in PVT Compared to Hällered and CFD* Master thesis performed at Volvo Cars, Linköpings Universitet, 2011
- [10] Mattias Eng *Investigation of Aerodynamic correction methods applied to a slotted wall Wind Tunnel* Master Thesis performed at Volvo Cars, Technische Universität Berlin, 2009
- [11] Stephane Cyr, Kang-Duck Ih & Sang-Hyun Park *Accurate Reproduction of Wind-Tunnel Results with CFD* Technical Paper 2011-01-0158, 2011
- [12] R. H. Barnard *Road Vehicle Aerodynamic Design, An Introduction* 2nd edition, Me-shaero Publishing 2001
- [13] S. Perzon *On Blockage Effects in Wind Tunnels - A CFD study* Technical Paper 2001-01-0705, 2001
- [14] O. Fischer, T. Kuthada, N. Widdecke & J. Wiedemann *CFD Investigations of Wind Tunnel Interference Effects* Technical Paper 2007-01-1045, 2007